Photocontrol of Protein Activity in Cultured Cells and Zebrafish with One- and Two-Photon Illumination

Deepak Kumar Sinha, Pierre Neveu, Nathalie Gagey, Isabelle Aujard, Chouaha Benbrahim-Bouzidi, Thomas Le Saux, Christine Rampon, Carole Gauron, Bernard Goetz, Sylvie Dubruille, et al.

Photocontrol of protein activity in cultured cells and zebrafish with one- and two-photon illumination[**]

Deepak Kumar Sinha,[a] Pierre Neveu,[a],[b],[i] Nathalie Gagey,[b] Isabelle Aujard,[b] Chouaha Benbrahim-Bouzidi,[b] Thomas Le Saux,[b] Christine Rampon,[c],[d] Carole Gauron,[c] Bernard Goetz,[b] Sylvie Dubruille,[e] Marc Baaden,[f] Michel Volovitch,[c],[g] David Bensimon,[a],[h],* Sophie Vriz,[c],[d],* Ludovic Jullien[b],*

[a] *Dr. D. K. Sinha, Dr. P. Neveu, Dr. D. Bensimon,*
Ecole Normale Supérieure, Département de Physique and Département de Biologie,
Laboratoire de Physique Statistique UMR CNRS-ENS 8550,
24 rue Lhomond, F-75231 Paris, France,
E-mail: David.Bensimon@ens.fr

[b] *Dr. P. Neveu, Dr. N. Gagey, Dr. I. Aujard, C. Benbrahim, Dr. T. Le Saux, B. Goetz, Prof. Dr. L. Jullien,*
Ecole Normale Supérieure, Département de Chimie,
UMR CNRS-ENS-UPMC Paris 06 8640 PASTEUR,
24, rue Lhomond, 75231 Paris Cedex 05, France,
E-mail: Ludovic.Jullien@ens.fr

[c] *Dr. C. Rampon, C. Gauron, Prof. Dr. M. Volovitch, Prof. Dr. S. Vriz*
Collège de France, UMR 8542 CNRS-ENS-CDF,
11 place M. Berthelot, F-75231 Paris Cedex 05, France.

[d] *Dr. C. Rampon, Prof. Dr. S. Vriz*
Université Paris Diderot – Paris 7, France.
80, rue du Général Leclerc Bat G. Pincus, 94276 Le Kremlin-Bicêtre Cedex, France,
E-mail: vriz@univ-paris-diderot.fr

[e] *S. Dubruille*
Institut Curie, UMR 176 Institut Curie-CNRS,
26, rue d'Ulm, 75005 Paris, France

[f] *Dr. M. Baaden*
Institut de Biologie Physico-Chimique, Laboratoire de Biochimie Théorique, CNRS UPR 9080,
13, rue Pierre et Marie Curie, F-75005 Paris, France.

[g] *Prof. Dr. M. Volovitch*
Ecole Normale Supérieure, Département de Biologie,
46, rue d'Ulm, 75231 Paris Cedex 05, France.

[h] *Dr. D. Bensimon*
Department of Chemistry and Biochemistry, UCLA, Los Angeles, USA.

[i] *Dr. P. Neveu*
Kavli Institute for Theoretical Physics, University of California at Santa Barbara,
Santa Barbara CA 93106, USA.

November 3, 2009

Cells respond to external signals by modifying their internal state and their environment. In multicellular organisms in particular, cellular differentiation and intra-cellular signaling are essential for the coordinated development of the organism.[1] Revealing and understanding the spatio-temporal dynamics of these complex interaction networks is one of biology major goals. While some of the most important players of these networks have been identified, much less is known of the quantitative rules that govern their interaction with one another and with other cellular components (affinities, rate constants, strength of non linearities such as feedback or feedforward loops, etc.). Investigating these interactions (a prerequisite before understanding or modeling them) requires the development of means to control or interfere spatially and temporally with these processes.

To address these issues, various approaches have been introduced to control protein activity. A first strategy relies on tuning protein concentration, by controlling gene expression or messenger RNA translation. This goal can be achieved with conditional gene expression systems[2] or by using antisense oligonucleotides.[3] However such a control introduces delays associated to mRNA or protein syntheses that prevent interfering with protein patterns at the time scale of fast biological processes such as phosphorylations.[4] A second strategy avoids this drawback by directly acting at the protein level: the activity of the protein of interest is restored with an appropriate stimulus. The fast spatio-temporal dynamics of photoactivation methods have proved particularly attractive. In favorable cases, photoactivable substrates can be used to alter the function of native or engineered proteins.[5] Direct caging of peptides and proteins has been reported by many groups.[6] However the caged precursors of these macromolecules must be injected into the cells, limiting their range of access. Genetically encoded photoactivable proteins do not suffer from this drawback in transgenic organisms. They can be designed to intrinsically bear the photoactive trigger.[7] Alternatively, they can contain a non-photoactive site which can be activated by a small permeant caged lipophilic molecule (such as derived from estradiol,[8] ecdysone,[9] 4-hydroxy tamoxifen [10, 11], or doxycycline[12]). This method has been successfully implemented to photo-control gene expression in eukaryotic systems with one- and two-photon excitation.[8, 9, 11, 12]

In the present study, we retained the principle of a small lipophilic caged inducer to photo-activate properly engineered proteins *in vivo*. We adopted a steroid-related inducer since various proteins (e.g. Engrailed, Otx2, Gal4, p53, kinases such as Raf-1, Cre and Flp recombinases) fused to a steroid receptor were shown to be activated by binding of an appropriate ligand (Scheme 1).[13] In its absence, the receptor forms a cytoplasmic assembly with a chaperone complex, inactivating the fusion protein.[14] Its function is restored in the presence of the steroid ligand which binds to the receptor and disrupts the complex. Like Link et al.,[11] we chose to photocontrol the activity of a target protein by fusing it to the extensively used modified estrogen receptor

ligand-binding domain (ER^{T2}) specific for the non-endogenous 4-hydroxy-tamoxifen (tamoxifen-OH) inducer.[15] In the present paper, we report on photocontrol over nuclear translocation of GFP-nls-ER^{T} and mCherry-nls-ER^{T}, two fluorescent proteins linked to the ER^{T2} receptor by a nuclear localization signal.

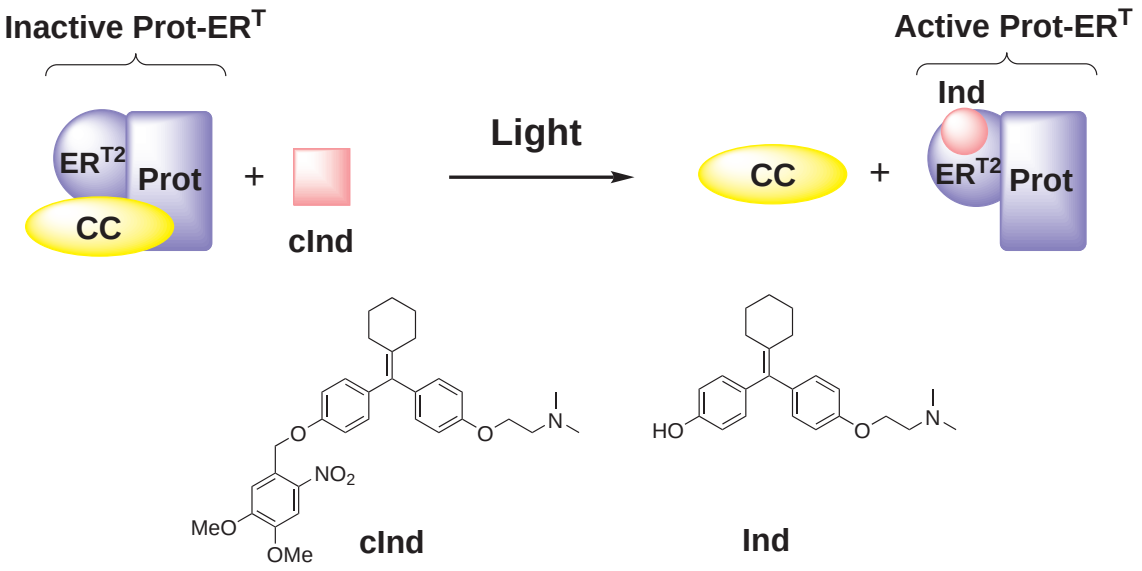

Scheme 1. A protein fused to the ER^{T2} receptor is inactivated by the assembly formed with a chaperone complex. Upon photoactivation of a caged precursor (**cInd**), a non-endogenous inducer (**Ind**, 4-hydroxy-cyclofen) is released, binds to the ER^{T2} receptor and sets the protein fusion free from its assembly with the chaperone complex.

Since we observed that tamoxifen-OH was susceptible to photo-isomerization and photo-degradation upon UV illumination at uncaging time scales (see Supporting Information), we looked for another inducer structurally related to tamoxifen-OH but which would not isomerize nor degrade upon UV illumination. In view of its synthetic accessibility, we adopted the core motif of the estrogen cyclofenil.[16] After grafting on one of its phenol groups the basic pendant chain present in tamoxifen-OH, we obtained 4-hydroxy-cyclofen (cyclofen-OH or **Ind**; Scheme 1) which was suggested from molecular dynamics simulations to be as active in binding the estrogen receptor as tamoxifen-OH (see Supporting Information). **Ind** was easily synthesized in two steps (Figure 3S): 4,4'-hydroxybenzophenone and cyclohexanone were first coupled under Mc Murry conditions (85 % yield) [17] and the resulting diphenol was subsequently monoalkylated with 2-(dimethylamino)ethyl chloride hydrochloride (40 % yield) to provide the targeted compound.

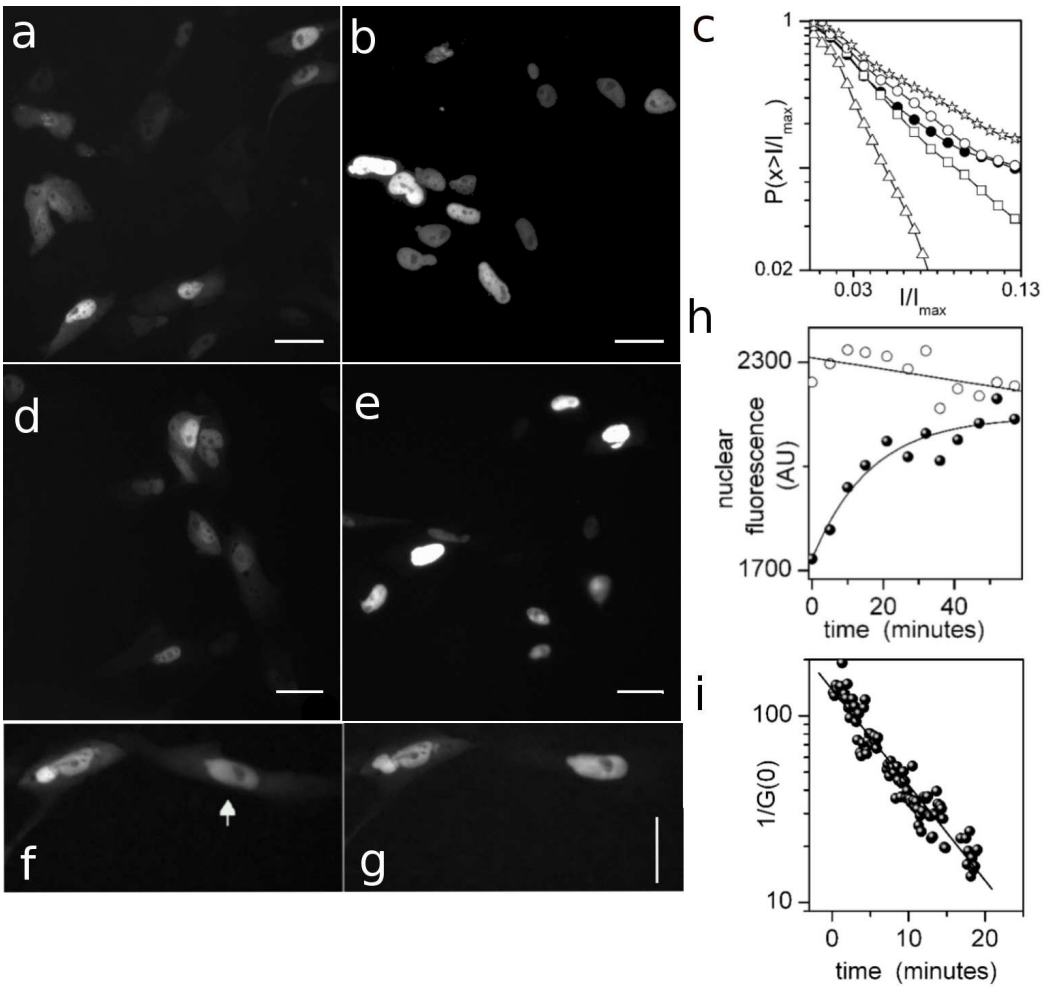

Figure 1. Induction of nuclear translocation of GFP-nls-ER$^{\mathrm{T}}$ by addition (**a**–**c**) or photorelease (**d**–**i**) of cyclofen-OH in CV1 cells transfected with a *gfp-nls-ER^{T}* plasmid. **a**–**c**: GFP fluorescence image of CV1 cells 24 h after transfection and further incubation with 0 (**a**) or 3 (**b**) μM **Ind** for 1 h (identical display range in **a** and **b**). **c**: Cumulative distribution of the mean nuclear intensity after 0.0 (triangles), 0.3 (squares), 3.0 (circles) and 5.0 (stars) μM **Ind** or 3.0 μM (disks) tamoxifen-OH treatment; **d**–**e**: GFP fluorescence image of CV1 cells imaged 24 h after transfection and further incubation in 6 μM **cInd** for 30 min without (**d**) and with (**e**) global 365 nm UV illumination; **f**–**h**: Selective nuclear GFP-nls-ER$^{\mathrm{T}}$ translocation in one cell (indicated by an arrow in **f**) upon two photon illumination (750 nm, 10 mW for 10 s): compare the fluorescence levels in the cytoplasm and in the nucleus of the targeted cell 0 (**f**) and 60 (**g**) min after illumination, using the nearby non-illuminated cell as a reference. **h**: Time evolution of the mean nuclear fluorescence intensity in the targeted cell (disks) and reference cell (circles) shown in (**f**–**g**); **i**: Time dependence of the value of the FCS autocorrelation curves at $\tau = 0$ in a CV1 cell incubated in 6 μM **cInd** for 30 min and illuminated for 5 s with a UV laser (375 nm, 5 μW). In **h** and **i**, dots: experimental data; solid lines: exponential fits (see Supporting Information). Same display range in **d**–**e** and in **f**–**g**. Scale bar: 10 μm.

First we tested cyclofen-OH in CV1 cells transfected with a plasmid expressing a *gfp-nls-ER^{T}* gene. When observed by epifluorescence microscopy 24 h later (Figure 1a), these cells displayed a weak cytoplasmic fluorescence background with occasional nuclear fluorescence. Addition of cyclofen-OH (or tamoxifen-OH) in the cell culture medium resulted in the disappearance of cy-

toplasmic fluorescence and a strong increase in nuclear fluorescence without alteration of the cell morphology (Figure 1b). As expected, the release upon ligand binding of GFP-nls-ER^T from its cytoplasmic chaperone complex permitted its nuclear translocation. We measured the cumulative distribution of nuclear fluorescence intensities (see Figure 1c and Supporting Information). In the absence of ligand, that probability differed significantly from zero only at low fluorescence intensities. Upon addition of cyclofen-OH, the fraction of cells displaying strong nuclear fluorescence increased with the concentration of ligand. Noticeably, the data revealed that cyclofen-OH and tamoxifen-OH induced similar fluorescence distributions at 3 μM of ligand (Figure 1c), a similarity expected from the molecular dynamics simulations of their binding to the ER^{T2} receptor. Thus it appears that cyclofen-OH is non-toxic and as efficient as tamoxifen-OH in binding to the ER^{T2} receptor of the GFP-nls-ER^T protein and in activating its nuclear translocation.

When aiming to photo-control the activity of proteins in a live animal, zebrafish (*Danio rerio*) is a system of choice due to its transparent embryo and existing lines without pigments. In fact, zebrafish has become a popular vertebrate model for developmental studies [18] and the investigation of human pathologies.[19] We checked that zebrafish embryos developed normally when incubated in various concentrations of cyclofen-OH (up to 5 μM) and displayed similar response as cell cultures when a GFP-nls-ER^T (or mCherry-nls-ER^T) mRNA was injected (at the one-cell stage): in absence of ligand, the embryos displayed a very weak overall fluorescence signal at 30 hours post fertilization (hpf) (Figure 2a and 5Sa). Upon incubation in a medium containing the ligand, the percentage of positive embryos (defined as those exhibiting nuclear fluorescence at 24 hpf) increased (Figure 2b and 5Sb), reaching 50 % at an inducer concentration $C_{1/2} = 0.2$ μM (Figure 2c and Table 2S).

Following the validation of cyclofen-OH as an efficient ER^{T2} ligand and its possible use to control protein activity in cell cultures and zebrafish embryos, we caged it with 4,5-dimethoxy-2-nitrobenzyl alcohol, 6-bromo-7-hydroxy-4-hydroxymethylcoumarin [20] and 7-dimethylamino-4-hydroxymethylcoumarin [21] under Mitsonobu conditions to give **cInd**, **c'Ind**, and **c"Ind** with 64 %, 45 %, and 32 % yields respectively (Scheme 1 and Figure 3S). We characterized *in vitro* the uncaging of these compounds by using high pressure liquid chromatography (HPLC) coupled to mass spectrometry to measure the temporal dependence of the concentration of photoreleased cyclofen-OH. With UV illumination at 365 nm, we observed that the inducer **Ind** could be photoreleased quantitatively from its three caged precursors **cInd**, **c'Ind**, and **c"Ind** with characteristic times of 270 s, 120 s, and 620 s respectively corresponding to uncaging cross sections at 365 nm of 22, 47, and 10 $M^{-1}cm^{-1}$ (see Supporting Information). We checked that the **cInd** and **c"Ind** caged precursors were inert in the dark and led to photocontrol in zebrafish embryos upon UV illumination. In contrast, **c'Ind** led to protein activation in zebrafish embryos, even in the absence of illumination. In the following we will focus on the easily accessible **cInd**. We showed

that cyclofen-OH could be released from **cInd** with two-photon illumination at 750 nm with an uncaging cross section equal to 4 mGM, in agreement with values reported for the photolabile 4,5-dimethoxy-2-nitrobenzyl protecting group.[20, 22]

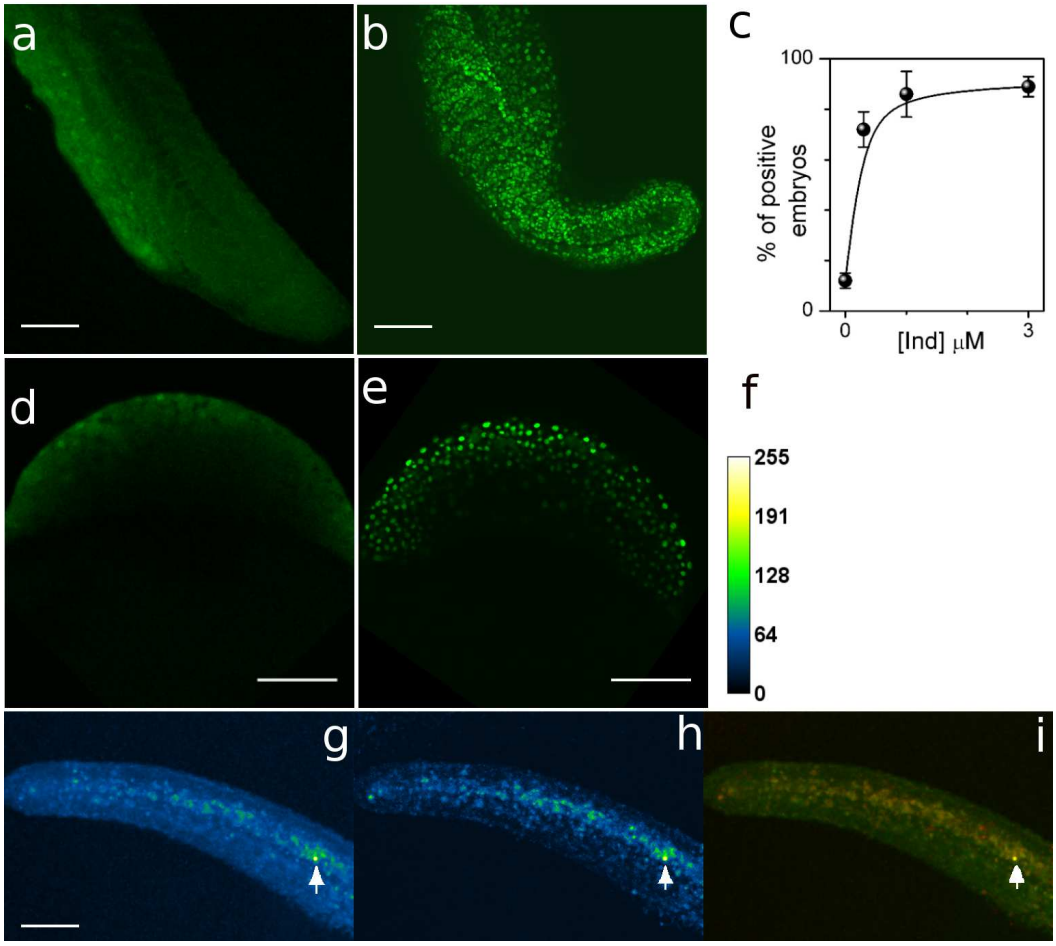

Figure 2. Induction of nuclear translocation of GFP-nls-ER$^{\mathrm{T}}$ by addition (**a**–**c**) or photorelease (**d**–**i**) of cyclofen-OH in wild type zebrafish embryos injected with *gfp-nls-ER*^{T} mRNA (100 ng/μL) at the one-cell stage. GFP fluorescence image of embryos at 24–30 hpf after incubation with 0 (**a**) or 3 (**b**) μM **Ind**; **c**: Dependence of the efficiency of nuclear translocation of GFP-nls-ER$^{\mathrm{T}}$ on inducer concentration. Error bars are statistical errors estimated as $\sqrt{p(1-p)/n}$ where p is the percentage of embryos exhibiting a positive phenotype and n is the total number of embryos investigated. The solid line is a guideline for the eyes; **d**–**e**: Confocal GFP fluorescence image of embryos at 4 hpf (following incubation at 2 hpf for 90 min in 3 μM **cInd** and washing) without illumination (**d**) and 30 min after illumination with UV light (**e**); **f**–**i**: Images resulting from local photoactivation (750 nm, 10 mW, 10 s) of GFP-nls-ER$^{\mathrm{T}}$ and mCherry-nls-ER$^{\mathrm{T}}$ in the tail at 24 hpf in a wild type embryo injected with their mRNA at one-cell stage and incubated from the dome stage to 24 hpf in embryo medium supplemented with 3 μM **cInd** and subsequent washing. GFP (**g**) and mCherry (**h**) intensity coded images (**f**) and their superposition (**i**). Scale bar: 100 μm.

In the absence of UV illumination, the fluorescence of CV1 cells transfected with a plasmid carrying a *gfp-nls-ER*^{T} gene incubated in 6 μM **cInd** for 30 min was essentially the same as that observed in cells incubated without inducer (compare Figures 1a and 1d). This result showed that the caged ligand **cInd** was inactive and non-toxic. On the other hand, when **cInd** was illuminated

by UV for a duration similar to its uncaging time, the cells displayed the characteristic nuclear fluorescence they show in the presence of ligand (compare Figures 1b and 1e). We also used short light pulses emitted by a 365 nm UV laser or by a Ti-Sa laser at 750 nm in a non-detrimental power regime (5 s at 5 μW and 10 s at 10–20 mW at the sample respectively) to photorelease **Ind** and induce the translocation of GFP-nls-ER$^{\mathrm{T}}$ in a single cell with one- and two-photon excitation respectively (Figures 1f and 1g and Supporting Information). In all cases, the cytoplasm and the nucleus of the targeted cell exhibit significant brightness changes with regard to surrounding cells: they become dimmer and brighter respectively. Figure 1h shows that the average nuclear fluorescence intensity of a targeted cell increases exponentially with time, leading to an estimate of the nuclear translocation time τ_{int}=1000±300 s (see Supporting Information). We also studied the kinetics of translocation from the Fluorescence Correlation Spectroscopy (FCS) signal of the cytoplasmic GFP-nls-ER$^{\mathrm{T}}$. We recorded time-series of FCS curves following uncaging of **cInd** (6 μM) in targeted cells. The FCS curves were globally fitted by assuming the cytoplasm to contain two GFP-nls-ER$^{\mathrm{T}}$ states: free and bound to a chaperone complex. We obtained satisfactory fits with diffusion coefficients $D_{bound} \simeq 0.1$ μm^{2}s^{-1} and $D_{free} \simeq 18.5$ μm^{2}s^{-1}, in line with expected orders of magnitude (see Supporting Information). From the value of the FCS curves at $\tau = 0$ which is inversely proportional to the number of cytoplasmic GFP-nls-ER$^{\mathrm{T}}$ molecules, we could show that their number drops exponentially upon nuclear translocation with a time scale τ_{int}=450±20 s (see Supporting Information) that is in the same order of magnitude as the value deduced from the increase in nuclear fluorescence and in line with published estimates.[23]

We then investigated the photo-induction of nuclear translocation in live zebrafish embryos. Wild type embryos were injected with *gfp-nls-ER^T* mRNA at one-cell stage and incubated (at 1 to 2 hpf) for 90 min in embryo medium supplemented with 3 μM **cInd**. As observed in cell cultures, **cInd** was inactive and non-toxic. In comparison with embryos incubated in regular medium, it did not induce a significantly larger GFP nuclear translocation and mortality (see Figure 2d and Table 3S). Upon uncaging of **cInd** by UV illumination of the whole embryo at 4–5 hpf, a global nuclear translocation of the GFP fused-protein was observed, in line with the cell culture data (Figure 2e). We studied in more details the dependence of GFP nuclear translocation on the duration of UV illumination (Table 3S and Figure 7S). As anticipated, the translocation yield increased with illumination duration. Using the dependence observed in Figure 2c for calibration, the data also suggested that the concentration of **cInd** in the embryo was in the same range as its concentration in the incubation solution.

Finally, we performed two colocalization experiments to verify that the control of protein activity did occur in the targeted illuminated cells only. We first used a UV laser to photoactivate caged Fluorescein dextran and **cInd** in wild type embryos injected with *gfp-nls-ER^T* mRNA and caged Fluorescein dextran at one-cell stage and incubated in embryo medium supplemented

with 3 μM **cInd**. As shown in the Supporting Information, the targeted cells only display a cytoplasmic fluorescence arising from fluorescein together with a GFP nuclear fluorescence signal. We performed a second colocalization experiment with two-photon illumination. Figures 2f–i display the distribution of fluorescence intensity in a wild type embryo injected with *gfp-nls-ER^T* mRNA and *mcherry-nls-ER^T* mRNA at one-cell stage. After incubation from the dome stage to 24 hpf in embryo medium supplemented with 3 μM **cInd** and subsequent washing, the embryo was illuminated at 24 hpf in the tail for 10 s with a Ti-Sa laser (750 nm, 10 mW). After 60 min, one observes a marked increase of fluorescence emission from a single nucleus which is in line with the cyclofen induction of nuclear translocation of both GFP-nls-ER$^{\mathrm{T}}$ (see also the 3D-reconstruction in the Supporting Information) and mCherry-nls-ER$^{\mathrm{T}}$ in a single cell of the embryo. This last observation bears much significance in evaluating the opportunities for photocontrol of protein activity down to the single cell level using the present approach. Equipped with the **Ind** dose response calibration curve in Figure 2c, the relevant photochemical information, and an estimate of the **cInd** concentration within the embryo (*vide supra*), one can set the two-photon illumination conditions to deliver and tune the concentration of cyclofen in the targeted cell to about $C_{1/2}$. Any leakage of the delivered inducer would be at too low a concentration to induce protein activity in neighboring cells.

We have shown that photo-releasing 4-hydroxy-cyclofen from a caged precursor is an efficient strategy to restore the function and investigate the fast dynamics of a protein fused to the ER$^{\mathrm{T2}}$ receptor in a zebrafish embryo. Compatible with a wide variety of proteins, the present non-invasive optical method could open up opportunities for the local spatio-temporal investigation of developmental pathways, the identification of stem cells and the study of cancer in a live organism, down to the single (or few) cell level, as suggested by the colocalization experiments.[24]

Supporting Information can be found online.

[**] This work has been supported by the ANR (PCV 2008, Proteophane), the NABI CNRS-Weizmann Institute program (for a fellowship to D.K.S.), and the Ministère de la Recherche (for fellowships to N.G. and P.N.). P.N. is supported in part by the National Science Foundation under Grant No. PHY05-51164. D. B. acknowledges partial support of a PUF ENS-UCLA grant. M. B. thanks ANR for support (Project ANR-06-PCVI-0025). The authors thank P. Leclerc and B. Matthieu for their kind help with confocal imaging. They are also thankful to Dr. V. Jullien and Prof. G. Pons at Service de Pharmacologie Clinique, Saint Vincent de Paul Hospital Paris, for access to their HPLC-MS instrument. The authors thank Dr. D. Metzger (IGBMC, Strasbourg, France) for providing the original plasmid containing the ER^{T2} coding sequence. G. Levkowitz is acknowledged for a generous gift of caged Fluorescein dextran. The authors declare no competing financial interests.

References

[1] J. Gerhart, M. Kirschner, *Cells, embryos, and evolution*, Blackwell science, **1997**.

[2] A. D. S. Ryding, M. G. F. Sharp, J. J. Mullins, *J. Endocrin.*, **2001**, *171*, 1–14.

[3] S. Karkare, D. Bhatnagar, *Appl. Microbiol. Biotechnol.*, **2006**, *71*, 575–586.

[4] a) A. Fujioka, K. Terai, R. E. Itoh, K. Aoki, T. Nakamura, S. Kuroda, E. Nishida, M. Matsuda, *J. Biol. Chem.*, **2006**, *281*, 8917–8926; b) J. Dengjel, V. Akimov, J. V Olsen, J. Bunkenborg, M. Mann, B. Blagoev, J. S Andersen, *Nat. Biotech.*, **2007**, *25*, 566–568.

[5] a) M. Volgraf, P. Gorostiza, R. Numano, R. H. Kramer, E. Y. Isacoff, D. Trauner, *Nat. Chem. Biol.*, **2006**, *2*, 47–52; b) P. Neveu, I. Aujard, C. Benbrahim, T. Le Saux, J.-F. Allemand, S. Vriz, D. Bensimon, L. Jullien, *Angew. Chem. Int. Ed.*, **2008**, *47*, 3744–3746.

[6] a) *Dynamic studies in biology*, M. Goeldner, R. Givens Eds, Wiley-VCH, Weinheim, **2005**; b) G. Mayer, A. Heckel, *Angew. Chem. Int. Ed.*, **2006**, *45*, 4900–4921; c) G. C. R. Ellis-Davies, *Nat. Meth.*, **2007**, *4*, 619–628; d) H.-M. Lee, D. R. Larson, D. S. Lawrence, *ACS Chem. Biol.*, **2009**, *4*, 409–427; e) A. Specht, F. Bolze, Z. Omran, J.-F. Nicoud, M. Goeldner, *HFSP J.*, **2009**, *3*, 255–264.

[7] a) F. Zhang, L.-P. Wang, M. Brauner, J. F. Liewald, K. Kay, N. Watzke, P. G. Wood, E. Bamberg, G. Nagel, A. Gottschalk, K. Deisseroth, *Nature*, **2007**, *446*, 633–641; b) Y. I. Wu, D. Frey, O. I. Lungu, A. Jaehrig, I. Schlichting, B. Kuhlman, K. M. Hahn, *Nature*, **2009**, *461*, 104–108.

[8] F. G. Cruz, J. T. Koh, K. H. Link, *J. Am. Chem. Soc.*, **2000**, *122*, 8777–8778.

[9] W. Y. Lin, C. Albanese, R. G. Pestell, D. S. Lawrence, *Chem. Biol.*, **2002**, *112*, 1347–1353.

[10] Y. Shi, J. T. Koh, *Chem. Bio. Chem.*, **2004**, *5*, 788–796.

[11] K. H. Link, Y. Shi, J. T. Koh,*J. Am. Chem. Soc.*, **2005**, *127*, 13088–13089.

[12] S. B. Cambridge, D. Geissler, F. Calegari, K. Anastassiadis, M. T. Hasan, A. F. Stewart, W. B. Huttner, V. Hagen, T. Bonhoeffer, *Nat. Meth.*, **2009**, *6*, 527–533.

[13] D. Picard,*Curr. Op. Biotech.*, **1994**, *5*, 511–515.

[14] a) J. Cheung, D. F. Smith,*Mol. Endo.*, **2000**, *14*, 939–946; b) D. Picard, *Trends in Endocrinology and Metabolism*, **2006**, *17*, 229–235; c) W. B. Pratt, Y. Morishima, Y. Osawa, *J. Biol. Chem.*, **2008**, *283*, 22885–22889.

[15] a) R. Feil, J. Brocard, B. Mascrez, M. LeMeur, D. Metzger, P. Chambon, *Proc. Nat. Acad. Sci. USA*, **1996**, *93*, 10887–10890; b) J. Brocard, X. Warot, O. Wendling, N. Messaddeq, J.-L. Vonesch, P. Chambon, D. Metzger, *Proc. Nat. Acad. Sci. USA*, **1997**, *94*, 14559–14563.

[16] C. B. Lunan, A. Klopper, *Clin. Endocrinol. (Oxford)*, **1975**, *4*, 551–572.

[17] M. M. Cid, J. A. Seijas, M. C. Villaverde, L. Castedo, *Tetrahedron*, **1988**, *44*, 6197–6200.

[18] a) R. T. Peterson, B. A. Link, J. E. Dowling, S. L. Schreiber, *Proc. Nat. Acad. Sci. USA*, **2000**, *97*, 12965–12969; b) P. J. Keller, A. D. Schmidt, J. Wittbrodt, E. H. K. Stelzer,*Science*, **2008**, *322*, 1065–1069.

[19] a) J. T. Shin, M. M. C. Fishman, *Annu. Rev. Genomics Hum. Genet.*, **2002**, *3*, 311–340; b) U. Langheinrich, *Bioessays*, **2003**, *9*, 904–912; c) G. E. Ackermann, B. H. Paw, *Front. Biosci.*, **2003**, *8*, 1227–1253; d) J. F. Amatruda, J. L. Shepard, H. M. Stern, L. I. Zon,*Cancer Cell*, **2002**, 229–231.

[20] T. Furuta, S. S.-H. Wang, J. L. Dantzker, T. M. Dore, W. J. Bybee, E. M. Callaway, W. Denk, R. Y. Tsien, *Proc. Nat. Acad. Sci. USA*, **1999**, *96*, 1197–1200.

[21] V. R. Shembekar, Y. Chen, B. K. Carpenter, G. P. Hess, *Biochemistry*, **2005**, *44*, 7107–7114.

[22] a) E. B. Brown, J . B. Shear, S. R. Adams, R. Y. Tsien, W. W. Webb, *Biophys. J.*, **1999**, *76*, 489–499; b) I. Aujard, C. Benbrahim, M. Gouget, O. Ruel, J. B. Baudin, P. Neveu, L. Jullien, *Chem. Eur. J.* **2006**, *12*, 6865–6879.

[23] a) N. Shulga, P. Roberts, Z. Gu, L. Spitz, M. M. Tabb, M. Nomura, D. S. Goldfarb, *J. Cell. Biol.* **1996**, *135*, 329–339; b) R. B. Kopito, M. Elbaum, *Proc. Natl. Acad. Sci. USA* **2007**, *104*, 12743–12748.

[24] P. Neveu, D. Sinha, P. Kettunen, S. Vriz, L. Jullien, D. Bensimon, *Single cell physiology* in *Nobel volume on Single Molecule Spectroscopy in Chemistry, Physics and Biology*, Springer, **2009**.

Suggestion for the Table of Contents

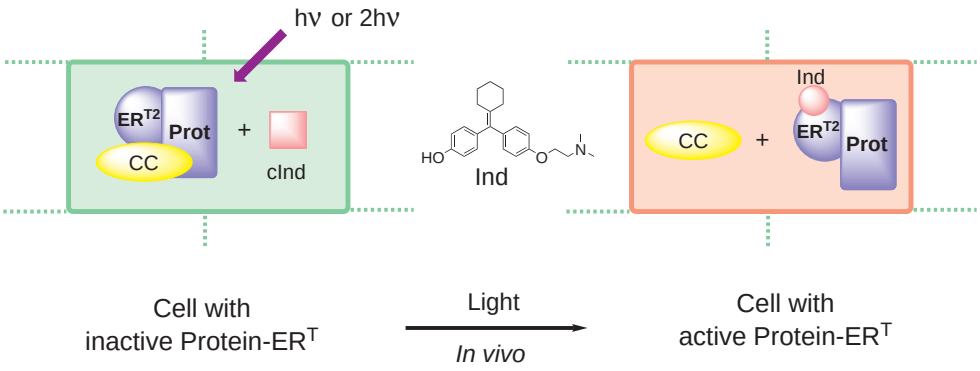

We use one- or two-photon illumination in cultured cells and in a live zebrafish embryo to uncage a precursor of a non-endogenous inducer that restores the activity of a protein fused to its binding domain. Here, the method is used to initiate the nuclear translocation of a fluorescent protein and investigate its kinetics. It could be used more generally to investigate other physiological processes with high spatio-temporal resolution.

Keywords: Caged compounds, Photolysis.

Photocontrol of protein activity in cultured cells and zebrafish with one- and two-photon illumination

Deepak Kumar Sinha,[a] Pierre Neveu,[a],[b],[i] Nathalie Gagey,[b] Isabelle Aujard,[b] Chouaha Benbrahim-Bouzidi,[b] Thomas Le Saux,[b] Christine Rampon,[c],[d] Carole Gauron,[c] Bernard Goetz,[b] Sylvie Dubruille,[e] Marc Baaden,[f] Michel Volovitch,[c],[g] David Bensimon,[a],[h],* Sophie Vriz,[c],[d],* Ludovic Jullien[b],*

[a] *Dr. D. K. Sinha, Dr. P. Neveu, Dr. D. Bensimon,*
Ecole Normale Supérieure, Département de Physique and Département de Biologie,
Laboratoire de Physique Statistique UMR CNRS-ENS 8550,
24 rue Lhomond, F-75231 Paris, France,
E-mail: David.Bensimon@ens.fr

[b] *Dr. P. Neveu, Dr. N. Gagey, Dr. I. Aujard, C. Benbrahim, Dr. T. Le Saux, B. Goetz, Prof. Dr. L. Jullien,*
Ecole Normale Supérieure, Département de Chimie,
UMR CNRS-ENS-UPMC Paris 06 8640 PASTEUR,
24, rue Lhomond, 75231 Paris Cedex 05, France,
E-mail: Ludovic.Jullien@ens.fr

[c] *Dr. C. Rampon, C. Gauron, Prof. Dr. M. Volovitch, Prof. Dr. S. Vriz*
Collège de France, UMR 8542 CNRS-ENS-CDF,
11 place M. Berthelot, F-75231 Paris Cedex 05, France.

[d] *Dr. C. Rampon, Prof. Dr. S. Vriz*
Université Paris Diderot – Paris 7, France.
80, rue du Général Leclerc Bat G. Pincus, 94276 Le Kremlin-Bicêtre Cedex, France,
E-mail: vriz@univ-paris-diderot.fr

[e] *S. Dubruille*
Institut Curie, UMR 176 Institut Curie-CNRS,
26, rue d'Ulm, 75005 Paris, France

[f] *Dr. M. Baaden*
Institut de Biologie Physico-Chimique, Laboratoire de Biochimie Théorique, CNRS UPR 9080,
13, rue Pierre et Marie Curie, F-75005 Paris, France.

[g] *Prof. Dr. M. Volovitch*
Ecole Normale Supérieure, Département de Biologie,
46, rue d'Ulm, 75231 Paris Cedex 05, France.

[h] *Dr. D. Bensimon*
Department of Chemistry and Biochemistry, UCLA, Los Angeles, USA.

[i] *Dr. P. Neveu*
Kavli Institute for Theoretical Physics, University of California at Santa Barbara,
Santa Barbara CA 93106, USA.

November 3, 2009

The Supporting Information reports on:

- The evaluation of the stability of estrogen receptor complexes with tamoxifen-OH and cyclofen-OH ligands via molecular dynamics simulations (including Figures 1S and 2S, and Table 1S).

- The Experimental Methods: the syntheses of cyclofen (**Ind**) and its caged variants (**cInd**, **c'Ind**, and **c"Ind**) (Figure 3S), the protocols for HPLC coupled to mass spectrometry, the methods for experiments in cells and zebrafish embryos, for image acquisition, for Fluorescence Correlation Spectroscopy and for uncaging experiments.

- The *in vitro* investigation by HPLC coupled to mass spectrometry of the photodegradation of 4-hydroxy-tamoxifen (Figure 4S).

- The cyclofen-induced control of nuclear translocation in zebrafish embryos: The cyclofen-induced nuclear translocation of mCherry-nls-ER^T in zebrafish embryos injected at one cell stage with *mcherry-nls-ER*^{T} mRNA (Figure 5S), the probability of observing the cyclofen-induced nuclear translocation of GFP-nls-ER^T as a function of inducer concentration (Table 2S).

- The uncaging kinetics of the caged inducers upon UV illumination *in vitro* and *in vivo*: The *in vitro* investigation by HPLC coupled to mass spectrometry of the uncaging kinetics upon UV illumination of **cInd**, **c'Ind**, and **c"Ind** (Figure 6S), the probability of nuclear translocation of GFP-nls-ERT as the duration of UV illumination in wild type zebrafish embryos incubated with **cInd** (Table 3S and Figure 7S).

- The uncaging kinetics of **cInd** with two-photon excitation.

- The kinetics of GFP-nls-ERT nuclear translocation after cyclofen uncaging derived from the increase in nuclear fluorescence intensity and from the FCS autocorrelation measurement of GFP fluorescence at various times after uncaging (Figures 8S and 9S).

- Colocalized activation of caged fluorescein-dextran and GFP-nls-ERT nuclear translocation upon illumination with a UV laser of an embryo incubated with **cInd** and caged fluorescein-dextran (Figure 10S).

- 3D-reconstruction of the cyclofen-photoinduced nuclear translocation of GFP-nls-ER^{T} in a single cell of a zebrafish embryo (3DGFPnlsERT.avi).

Evaluation of the stability of estrogen receptor complexes with tamoxifen-OH and cyclofen-OH ligands via molecular dynamics simulations

To get some insight about the interaction of the cyclofen-OH putative inducer with the modified estrogen receptor (ER^{T2}), we performed several Molecular Dynamics (MD) simulations[1] using tamoxifen-OH as a reference. In the absence of any crystal structure of the tamoxifen-OH:ER^{T2} complex, we decided to analyze the interaction of both cyclofen-OH and tamoxifen-OH with the steroid receptor ERα mutated to adopt the ER^{T2} sequence (Gly400Val, Met543Ala, Leu544Ala; subsequently referred to as the reference REF), starting from the 2.0 Å crystal structure of the ERα ligand-binding domain complexed with lasofoxifene,[1] a compound structurally closely related to tamoxifen (and tamoxifen-OH). We investigated the interaction of tamoxifen-OH and of cyclofen-OH with the reference REF ligand-binding domain (simulations T1 and C1 respectively). We also analyzed the interaction of cyclofen-OH with the REF D351E mutant, in order to assess whether a slightly longer acidic side-chain at position 351 might benefit binding (simulation C2).

All MD simulations lead to stable ligand-binding domain/ligand complexes. The time evolution of the root mean square displacements (RMSD) of the protein reaches a stable plateau between 10 and 20 ns (data not shown).[2] Figure 1S shows representative snapshots of the three simulations. The ligands are firmly inserted in their binding pockets and are in very similar orientations for T1, C1 and C2. In particular, in the detailed view of the C1 binding pocket and ligand orientation shown in Figure 1Sc, the cyclofen-OH ligand positions itself similarly to other known ERα ligands.[1] In addition, it remains solvent accessible via two accessibility sites: a large cleft, which could serve ligand binding and unbinding, and a channel that might enable solvent to hydrate the binding site.

[1] Molecular dynamics (MD) simulations were run for 30 ns with the YASARA program.[2] Force-field parameterization for tamoxifen-OH and cyclofen-OH ligands was carried out using the AutoSMILES procedure, otherwise the AMBER99 forcefield was used.[3] All systems were solvated with 7936 explicit TIP3P water molecules and 20 Na^+ and 22 Cl^- counterions were added as background salt and to preserve overall electrical neutrality. Each system was energy minimized using the steepest descent method to relax any steric conflicts before beginning the simulations. Simulations were carried out with periodic boundary conditions. Long-range electrostatic interactions were calculated using PME with a direct-space cut-off of 7.86 Å. All simulations were performed using an NVT ensemble at 298 K. A 2fs/1fs double integration time step was used. Graphics were prepared with VMD.[4] Standard conformational analysis was carried out using YASARA, Gromacs tools[5] and locally written code. Statistical and data analysis was performed using the R statistical software package[6] and Xmgrace.[7]

[2] The actual RMSD values are low, with C1 showing the least deviations (1.4 Å) and the reference simulation T1 being around 2 Å RMSD. The mutant C2 shows a slightly higher RMSD (2.9 Å) induced by the introduction of a longer sidechain at position 351.

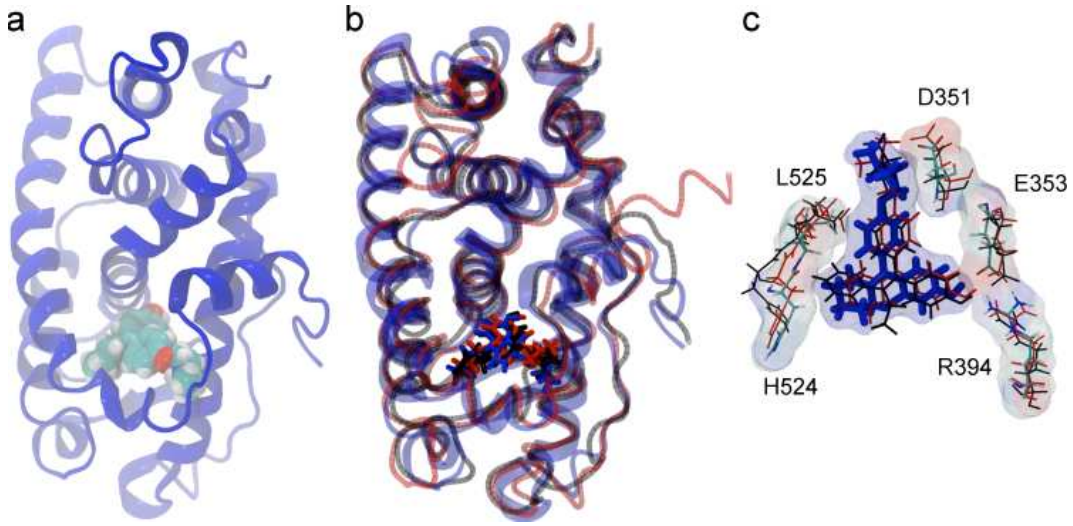

Figure 1S. MD simulation snapshots. **a**: Representative structure of simulation C1 highlighting the position of the cyclofen-OH ligand within the ligand-binding domain; **b**: Superposition of representative ligand-binding domain/ligand complexes from simulations T1 (black), C1 (blue) and C2 (red); **c**: Zoom on the ligand binding site with key interacting residues (Arg 394, Glu 353, Asp 351, His 524, and Leu 525).

The stabilization of the ligand can be assessed via its contacts with the receptor as shown in Figure 2Sa. All three simulations yield very similar contacts over the last 10 ns of the simulation, with average values indicated in Table 1S. Another aspect of ligand stabilization concerns the number of hydrogen bonds formed with the receptor. This number varies between 0 and 3 as illustrated by Figure 2Sb. Average values are indicated in Table 1S, with C1 slightly above T1 and clearly above C2. The most stable hydrogen bond observed in all three simulations is between Glu 353 and the ligand OH group. The ligand amine group can also form hydrogen bonds, in particular with Asp 351 (simulation T1) or Met 528 (simulation C1). Eventually, we have carried out an estimation of the binding affinity between the ligand and the ligand-binding domain, based on the force-field interaction energies. The results were normalized with respect to the average binding affinity observed in reference simulation T1, which was set to zero. As illustrated by Figure 2Sc, the estimation undergoes important fluctuations during the simulation. Average values are indicated in Table 1S, showing that simulation C1 exhibits a slightly more favorable binding affinity compared to T1, whereas the mutant receptor in simulation C2 exhibits lower affinity.

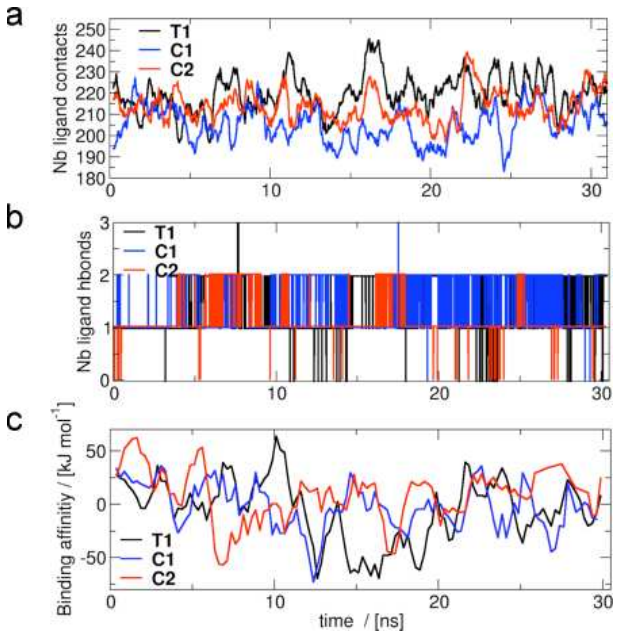

Figure 2S. Assessment of the ligand stabilization. Number of contacts (**a**) and hydrogen bonds (**b**) between protein and ligand. A contact was counted for each atom pair closer than 3.5 Å and hydrogen bonds were determined via Yasara based on an energy criterion; **c**: Estimated binding affinities for the various ligands. Simulations T1 (black), C1 (blue) and C2 (red).

Table 1S. Summary of the analysis carried out from MD simulations. The number of ligand - protein contacts and ligand - hydrogen bonds, as well as the binding affinity expressed in kJmol^{-1} have been averaged over the last ten nanoseconds of the simulation. The numbers in brackets indicate the standard deviation calculated as $\sigma = \sqrt{\frac{1}{N}\sum_{i=1}^{N}(x_i - \overline{x})^2}$.

Simulation	Ligand Contacts	Ligand H-bonds	Binding affinity (kJmol^{-1})
T1	221(18)	1.6(5)	0(35)
C1	214(18)	1.7(5)	-8(43)
C2	218(19)	1.0(2)	12(33)

As a conclusion, all structural analysis (comprising RMSD), observed binding mode, number of contacts and hydrogen bonds extracted from MD simulations suggest that the ER^{T2}/cyclofen-OH complex should exhibit comparable binding properties with respect to the reference tamoxifen-OH complex.

Experimental methods

Syntheses

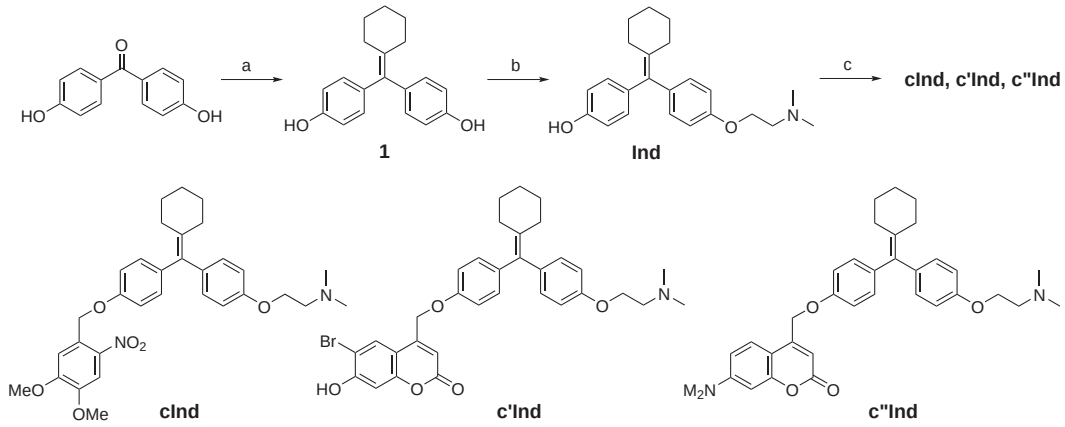

Figure 3S. Syntheses of 4-hydroxy-cyclofen **Ind** and its caged derivatives: a) cyclohexanone, $TiCl_4$, Zn, THF, reflux, 2 h; b) $Cl(CH_2)_2N(CH_3)_2.HCl$, K_2CO_3, acetone-H_2O, reflux, 18 h; c) caging alcohol, $P(Ph)_3$, diisopropylazodicarboxylate, THF, sonication, 20 min.

General Information

4,5-Dimethoxy-2-nitrobenzyl alcohol was purchased from Sigma. 6-Bromo-7-hydroxy-4-hydroxymethylcoumarin and 7-dimethylamino-4-hydroxymethylcoumarin were synthesized according to published procedures.[8, 9] Commercially available reagents were used as obtained. Microanalyses were performed by the Service de Microanalyses de Gif sur Yvette. Melting points were determined with a Büchi 510 capillary apparatus. ^1H and ^{13}C NMR spectra were recorded at room temperature on Bruker AM 250 or 400 spectrometers; chemical shifts are reported in ppm with protonated solvent as internal reference (^1H, $CHCl_3$ in $CDCl_3$ 7.26 ppm, CHD_2OD in CD_3OD 3.31 ppm, CHD_2SOCD_3 in CD_3SOCD_3 2.49 ppm, CHD_2COCD_3 in CD_3COCD_3 2.05 ppm; ^{13}C, $^{13}CDCl_3$ in $CDCl_3$ 77.0, $^{13}CD_3OD$ in CD_3OD 49.1 ppm, $^{13}CD_3SOCD_3$ in CD_3SOCD_3 39.7 ppm, $^{13}CD_3COCD_3$ in CD_3COCD_3 29.9 ppm; coupling constants J are given in Hz. Mass spectra (chemical ionization and high resolution with NH_3 or CH_4) were performed by the Service de Spectrométrie de Masse de l'ENS (Paris). Column chromatography was performed on silica gel 60 (0.040-0.063 nm) Merck. Analytical thin-layer chromatography (TLC) was conducted on Merck silica gel 60 F_{254} precoated plates. HPLC analyses and purifications of the final caged species were performed on a Waters system incorporating a Wdelta 600 pump with a PDA 996 UV detector working at 245 nm (columns: analytical: X Terra Waters MS C18, 150 × 4.6 mm,

5 μm, 1 mL/min flow; preparative: X Terra Waters Prep MS C18, 150 × 19 mm, 5 μm, 12 mL/min flow; elution with solution A: water with 0.05 % formic acid and solution B: acetonitrile with 0.05 % formic acid).

4-(cyclohexylidene(4-hydroxyphenyl)methyl)phenol 1 [10]

Titanium chloride (6.2 mL, 56 mmol) was added dropwise under argon to a stirred suspension of zinc powder (8.20 g, 126 mmol) in dry tetrahydrofuran (80 mL) at -10°C. When the addition was complete, the mixture was warmed to room temperature and then refluxed for 2 h. A solution of 4,4'-hydroxybenzophenone (2.0 g, 9 mmol) and cyclohexanone (4 mL, 38 mmol) in dry tetrahydrofuran (120 mL) was added to the cooled suspension of the titanium reagent at 0°C and the mixture was refluxed for 2 h. After being cooled to room temperature, the reaction mixture was quenched with 10 % (w/v) aqueous potassium carbonate (30 mL), filtered and extracted with ethyl acetate. The organic layer was washed with brine, dried over $MgSO_4$, and concentrated *in vacuo*. Flash column chromatography (cyclohexane/ethyl acetate: 3/1 v/v) afforded **1** as a white powder (2.15 g, 85 %). ^{1}H NMR (250 MHz, DMSO-d_6) δ 9.28 (s, 2H), 6.82 (d, 4H, J=8.4 Hz), 6.65 (d, 4H, J=8.4 Hz), 2.14 (m, 4H), 1.52 (m, 6H); ^{13}C NMR (100 MHz, DMSO-d_6) δ 155.5, 136.2, 133.8, 133.6, 130.3, 114.6, 31.9, 28.1, 26.3.

4-((4-(2-(dimethylamino)ethoxy)phenyl) (cyclohexylidene)methyl)phenol Ind (4-hydroxy-cyclofen)

2-(Dimethylamino)ethyl chloride hydrochloride (256 mg, 1.78 mmol) was dissolved in a solution of acetone/water (19/1 v/v, 40 mL) and treated with potassium carbonate (600 mg, 4.4 mmol). The mixture was stirred at 0°C for 30 min. **1** (500 mg, 1.78 mmol) was dissolved in the above solution at 0°C and potassium carbonate (580 mg, 4.2 mmol) was added. The mixture was refluxed in the dark for 18 h. The solids were filtered off, and the filtrate was concentrated *in vacuo*. The crude product was purified by flash column chromatography (dichloromethane/methanol: 9/1 v/v) to afford **Ind** as a white powder (250 mg, 40 %). m. p. 180-181°C (methanol); ^{1}H NMR (250 MHz, $CDCl_3$) δ 6.95-6.89 (m, 4H), 6.70 (AA'XX', 2H, J=8.5 Hz), 6.59 (AA'XX', 2H, J=8.5 Hz), 4.04 (t, 2H, J=5.5 Hz), 2.82 (t, 2H, J=5.5 Hz), 2.40 (s, 6H), 2.25-2.21 (m, 4H), 1.57 (m, 6H); ^{13}C NMR (100 MHz, $CDCl_3$) δ 156.6, 154.7, 137.9, 136.1, 135.0, 133.5, 131.0, 130.8, 115.0, 113.5, 64.6, 58.1, 45.3, 45.2, 32.5, 32.4, 28.6, 26.8; MS (CI, CH_4): m/z 352 (calcd av mass

for $C_{23}H_{29}NO_2$: 351.22); MS (CI, CH_4, HR): m/z 352.2271 (calcd av mass for $C_{23}H_{30}NO_2$: 352.2277); $C_{23}H_{29}NO_2, 0.5H_2O$ (360.49): Anal. Calcd., C, 76.63; H, 8.39; N, 3.89; Found, C, 76.95; H, 8.09; N, 3.87.

2-(4-((4-(4,5-dimethoxy-2-nitrobenzyloxy)phenyl) (cyclohexylidene)methyl)phenoxy)-N,N-dimethylethanamine cInd [11]

A solution of **Ind** (180 mg, 0.5 mmol), 4,5-dimethoxy-2-nitrobenzyl alcohol (115 mg, 0.54 mmol) and triphenylphosphine (140 mg, 0.54 mmol) in tetrahydrofuran (0.25 mL) was sonicated for several minutes to allow for mixing. To the viscous resulting solution, diisopropylazodicarboxylate (0.106 mL, 0.54 mmol) was added dropwise while sonicating. After sonicating for 20 minutes, the reaction mixture was concentrated *in vacuo* and purified by column chromatography on silica gel with dichloromethane/methanol: 9/1 v/v as eluent to give **cInd** (180 mg, 64 %). m. p. 116-117°C (isopropylether, yellow cristals); ^{1}H NMR (400 MHz, $CDCl_3$) δ 7.76 (s, 1H), 7.35 (s, 1H), 7.04 (AA'XX', 2H, J=8.7 Hz), 7.00 (AA'XX', 2H, J=8.7 Hz), 6.90 (AA'XX', 2H, J=8.7 Hz), 6.82 (AA'XX', 2H, J=8. 7 Hz), 5.47 (s, 2H), 4.03 (t, 2H, J=5.8 Hz), 3.96 (s, 3H), 3.94 (s, 3H), 2.70 (t, 2H, J=5.8 Hz), 2.32 (s, 6H), 2.23 (m, 4H), 1.58 (m, 6H); ^{13}C NMR (100 MHz, $CDCl_3$) δ 157.0, 156.2, 153.8, 147.7, 138.9, 138.5, 136.8, 137.7, 133.2, 131.0, 130.7, 129.6, 114.3, 113.8, 109.4, 107.9, 67.0, 65.8, 58.3, 56.3, 56.3, 45.8, 32.4, 28.6, 26.8; $C_{32}H_{38}N_2O_6$ (546.66): Anal. Calcd., C, 70.32; H, 7.00; N, 5.12; Found, C, 70.11; H, 7.24; N, 5.02. After preparative HPLC purification (elution profile: 0–5 min: 50 % A and 50 % B; 5–15 min: 10 % A and 90 % B), **cInd** was shown by analytical HPLC to contain less than 2% residual of **Ind**.

4-((4-((4-(2-(dimethylamino)ethoxy)phenyl) (cyclohexylidene)methyl)phenoxy)methyl)-6-bromo-7-hydroxycoumarin c'Ind

Same as for **cInd** using **Ind** (110 mg, 0.31 mmol), 6-bromo-7-methoxymethoxy-4-hydroxycoumarin [12] (100 mg, 0.31 mmol), triphenylphosphine (86 mg, 0.33 mmol), diisopropylazodicarboxylate (0.065 mL, 0.33 mmol) and tetrahydrofuran (0.2 mL). After sonicating, trifluoroacetic acid (2 mL) was added and the mixture was stirred at room temperature for 15 min. The solvent was removed *in vacuo*. Purification by column chromatography with dichloromethane/methanol 9/1 v/v as eluent yielded **c'Ind** (60 mg, 30 %). ^{1}H NMR (250 MHz, DMSO-d_6) δ 8.00 (s, 1H), 7.09-6.75 (m, 9H), 6.39 (s, 1H), 5.33 (s, 2H), 4.06 (t, 2H, J=5.6 Hz), 2.75 (t, 2H, J=5.6 Hz), 2.32 (s, 6H), 2.17 (m, 4H), 1.55 (s, 6H); ^{13}C NMR (100 MHz, $CDCl_3$) δ 160.2, 157.0, 156.2,

155.8, 154.1, 149. 1, 138.7, 137.3, 135.6, 133.0, 131.0, 130.7, 127.5, 114.1, 113.8, 112.6, 111.9, 108.4, 104.0, 65.7, 65.5, 58.1, 45.7, 32.4, 28.6, 26.7; MS (CI, NH_3): m/z 606,604 (calcd av mass for $C_{33}H_{35}{}^{81}BrNO_5$: 606.19, $C_{33}H_{35}{}^{79}BrNO_5$: 604.16); MS (CI, NH_3, HR): m/z 606.1677 (calcd av mass for $C_{33}H_{35}{}^{81}BrNO_5$: 606.1684), 604.1693 (calcd av mass for $C_{33}H_{35}{}^{79}BrNO_5$: 604.1699). After preparative HPLC purification (elution profile: 0–5 min: 50 % A and 50 % B; 5–15 min: 10 % A and 90 % B), **c'Ind** was shown by analytical HPLC to contain less than 2% residual of **Ind**.

4-((4-((4-(2-(dimethylamino)ethoxy)phenyl) (cyclohexylidene)methyl)phenoxy)methyl)-7-dimethylaminocoumarin c"Ind

Same as for **cInd** using **Ind** (200 mg, 0.57 mmol), 7-(dimethylamino)-4-(hydroxymethyl)-2H-chromen-2-one [9] (125 mg, 0.57 mmol), triphenylphosphine (150 mg, 0.57 mmol), diisopropylazodicarboxylate (0.112 mL, 0.57 mmol) and tetrahydrofuran (0.3 mL). Purification by column chromatography with dichloromethane/methanol 9/1 v/v as eluent yielded **c"Ind** (100 mg, 32 %). ^{1}H NMR (250 MHz, $CDCl_3$) δ 7.38 (d, 1H, J=8.9 Hz), 7.04-6.74 (m, 8H), 6.61 (dd, 1H, J=2.4 and 8.9 Hz), 6.53 (d, 1H, J=2.4 Hz), 6.32 (s, 1H), 5.12 (s, 2H), 4.15 (t, 2H, J=5.2 Hz), 3.05 (s, 6H), 2.91 (t, 2H, J=5.2 Hz), 2.48 (s, 6H), 2.22 (m, 4H), 1.57 (m, 6H); ^{13}C NMR (63 MHz, $CDCl_3$) δ 161.9, 157.0, 156.2, 156.0, 152.8, 150.5, 138.6, 137.0, 135.8, 133.2, 131.0, 130.9, 124.3, 114.1, 1 13.9, 108.9, 107.7, 106.8, 98.4, 65.9, 65.7, 58.2, 45.7, 40.1, 32.5, 28.6, 26.8; MS (CI, CH_4): m/z 553 (calcd av mass for $C_{35}H_{41}N_2O_4$: 553.3; MS (CI, CH_4, HR): m/z 553.3065 (calcd av mass for $C_{35}H_{41}N_2O_4$: 553.3066). After preparative HPLC purification (elution profile: 0–50 min: 15 % A and 85 % B), **c"Ind** was shown by analytical HPLC to contain less than 2% residual of **Ind**.

HPLC coupled to mass spectrometry

High pressure liquid chromatography was carried out with an Accela System liquid chromatograph (Thermo Finnigan, Les Ulis, France) equipped with a Hypersil Gold column (1.9 μm x 2.1 x 50 mm) connected to a Thermo-Finnigan TSQ Quantum Discovery Max triple quadrupole mass spectrometer. 5 μL of sample solution was injected in the chromatographic column. For photodeprotection studies, the samples were eluted in isocratic mode at a flow rate of 400 μLmin^{-1} with a water-acetonitrile mixture (60 - 40 % v/v) containing 0.05 % formic acid. For the isomerization

study, the separation of isomers was carried out by gradient elution at a flow rate of 400 μLmin^{-1} from 5% to 95% water/methanol mixtures containing 0.05% formic acid in 20 min. Between each injection, the column was equilibrated with the mobile phase for 5 min. After separation, the analytes were introduced in the mass spectrometer through a heated electrospray ionization source (50°C) operating in the positive mode. The temperature of the capillary transfer was set at 270°C. Nitrogen was employed as nebulizing (35 psi) and auxiliary gas (30 arbitrary units). Argon was used as collision gas (1.0 milliTorr in Q2). 4-hydroxy-cyclofen (**Ind**) was observed (ion spray voltage of 3000 V) in the single reaction monitoring (SRM) mode (m/z 352.2 $\longrightarrow$72) using 30 V collision energy and 130 V tube lens . The stereoisomers of 4-hydroxytamoxifen and the corresponding dehydrophenanthrens (ion spray voltage of 3000 V) were followed in the single ion monitoring (m/z 388.3) mode using 175 V tube lens. All the possible settings were optimized by repetitive injections of the analyte in the chromatographic system. Instrument control and data collection were handled by a computer equipped with Xcalibur software (version 2.0).

Methods for experiments in cells and zebrafish embryos

Cell experiments

CV1 cells were plated on 35 mm Petri-dishes in 1 to 2 mL of incubation medium (10% FBS in DMEM) at a density of 100-200 cells/mm^2 and incubated at 37°C and 5% CO_2 24 hr before transfection. CV1 cells were transfected with 1 μg of plasmid with Lipofectamin (Invitrogen).

A detailed description of the cloning of the plasmids coding for *gfp-nls-ER^T* and *mcherry-nls-ER^T* is available on request.

To assay the effect of the various ligands or their caged precursors, CV1 cells were incubated at various concentrations of these substrates (0–5 μM) for different durations (15–60 min) and fixed in 4% PFA before imaging. In uncaging assays of **cInd**, the molecule was added 24 h post transfection for 15 to 30 min before illumination.

Expression of GFP-nls-ER^T was assayed 24 h after transfection by imaging the GFP fluorescence.

Zebrafish embryo experiments

Wild-type zebrafish embryos were injected at one-cell stage with appropriate mRNA synthesized with an *in vitro* transcription kit (mMessage mMachine, Ambion). They were subsequently

dechorionated by pronase treatment at dome stage prior to incubation in an aqueous solution of the various substrates (up to 30 hours post fertilization – hpf – with **Ind**, for 90 min with **cInd** except for the experiment displayed in Figure 2f–i where up to 24 hpf). **Ind** was photo-released from **cInd** 4–5 hpf (except in Figure 2f–i; 24 hpf). Illuminated embryos were observed 30 min (60 min in Figure 2f–i) after illumination for the GFP-nls-ER^{T} or mCherry-nls-ER^{T} fluorescence.

Embryos positive for either GFP nuclear translocation were scored under a microscope in a double-blind protocol.

Image acquisition and analysis

A fluorescence microscope (Olympus BX51WI) equipped with a Luca CCD Camera (Andor technologies) was used for image acquisition of the cells (filters: U-MWIBA3 Olympus for GFP and U-MWIG3 Olympus for mCherry). In a given series of experiments, all the conditions (EM-gain, exposure duration, lamp power etc) were identical to allow for a comparison of the observed fluorescence intensities. The images of embryos were acquired using confocal microscopes Leica TCS SP2 AOBS or Zeiss Axiovert 200M LSM510-Meta.

To draw Figure 1c, we analyzed the images recorded at all the **Ind** concentrations by extracting the average nuclear intensity I from each cell (at least 100 cells have been analyzed at each **Ind** concentration). We subsequently plotted the resulting histogram I/I_{max} after normalizing by the intensity I_{max} of the brightest cell nucleus across all the cells and all the **Ind** concentrations. The probability $P(x > I/I_{max})$ is obtained by integrating the histogram from 0 to I/I_{max} (cumulative distribution).

For the analysis of the phenotypes resulting in Figures 2c and 7S, we considered as positive embryos those embryos exhibiting a spotty fluorescence associated to fluorescence localized in the nuclei.

For the analysis of localization and colocalization of GFP and Fluorescein displayed in Figures 10Sa–c, we performed multichannel fluorescence imaging (excitation: 488 nm; emission channels: 500–512 nm, 512–522 nm and 530–600 nm). GFP and fluorescein signals were unmixed by using reference spectra acquired from embryos labeled with GFP or fluorescein only.

Fluorescence Correlation Spectroscopy

FCS was used (i) to characterize the focal points of the various objectives by analyzing the autocorrelation curves of 50 or 100 nM fluorescein solutions in 0.1 M NaOH (V_{exc}, the illuminated volume, from the value of the autocorrelation function at zero time using Fluorescein concentration and ω_{xy}, the beam waist, from the Fluorescein diffusion time using its known diffusion coefficient);[13] (ii) to analyze the kinetics of the nuclear translocation of GFP-nls-ER^{T}. For FCS experiments, illumination in the preceding microscope (Olympus BX51WI) was provided either by a 488 nm laser (Ar-ion, Spectra Physics) or by a mode-locked Ti-Sapphire laser (200 fs, 76 MHz, 750 nm; Mira, Coherent). The fluorescence photons were collected through filters (U-MWIBA3 set; without excitation filter, emission filter: BP460-495), dichroic mirrors (DM505 for 488 nm excitation and 700 short pass – Olympus for 750 nm excitation wavelengths) and optical fibers (FG200LCR multimode fiber, Thorlabs) and were detected with avalanche photodiodes (SPCM-AQR-14, Perkin Elmer) coupled to an ALV-6000 correlator (ALV GmbH). The incident powers at the sample were measured with a NOVA II powermeter (Laser Measurement Instruments). All the series of experiments reported in the present work have been performed in a regime of laser powers (3 to 5 μW for 488 nm and 5 to 20 mW for 750 nm) in which fluorescein exhibits a linear (with one-photon excitation) or quadratic (with two-photon excitation) dependence of the intensity of fluorescence emission on the illumination power.

Illumination experiments

With UV lamps

One-photon illumination experiments were performed at 20°C, with bench top UV lamps (365 nm, essentially a strong line at 365 nm accompanied by a gaussian spectral dispersion around 350 nm with a 40 nm width at half height; Fisher Bioblock) delivering typical 2.2 10^{-5} (4 W; *in vitro* experiments) and 4 10^{-5} (6 W; *in vivo* experiments) Einstein min^{-1} photon fluxes in the illuminated sample.[14]

We checked that, when illuminated for up to 4 min, the embryos developed normally. We also verified that the sideproduct resulting from uncaging **cInd** did not induce any noticeable morphological alterations in the embryo development.

With UV laser and two-photon excitation

A 40× 0.8 NA water immersion objective (Olympus) was used to image the embryos on a CCD camera (Andor Luca) and locate the focal spot of the UV laser/two-photon excitation. For the UV illumination (375 nm, CW, from Crystal Laser) a beam of 1 mm diameter was coupled to the microscope without expansion. For two photon illumination (200 fs, 76 MHz, 750 nm, provided by a mode-locked Ti-Sapphire laser (Mira, Coherent) the beam was expanded to $\sim$ 6 mm diameter to fill the back aperture of the objective. The incident power at the sample ($\sim$ 5 μW with the UV- and $\leq$ 20 mW with the IR-laser) was measured with a NOVA II powermeter (Laser Measurement Instruments).

The photodegradation of 4-hydroxy-tamoxifen may limit its use as a photoactivable molecule

4-hydroxy-tamoxifen has been caged with the 4,5-dimethoxy-2-nitrobenzyl photolabile protecting group and the resulting caged inducer has been successfully implemented to photocontrol gene expression in cultured cells with UV illumination.[15] Before designing and adopting 4-hydroxy-cyclofen as another related inducer, we used 4-hydroxy-tamoxifen for preliminary studies. In particular, we have been concerned with its possible photoisomerization and photodegradation after reading that the parent tamoxifen exhibited photoisomerization and photodegradation upon UV illumination.[16]

In a first experiment (data not shown), we illuminated a 25 μM solution of 4-hydroxy-tamoxifen in 1:1 (v:v) acetonitrile:water with the UV lamp and followed the temporal evolution of its absorption and fluorescence emission spectra. In particular, we observed in the fluorescence emission spectrum the growth of an emission band exhibiting similarities with the one of the phenanthren derivatives originating from illuminating tamoxifen.[16]. Hence this first experiment suggested that 4-hydroxy-tamoxifen experienced some photodegradation.

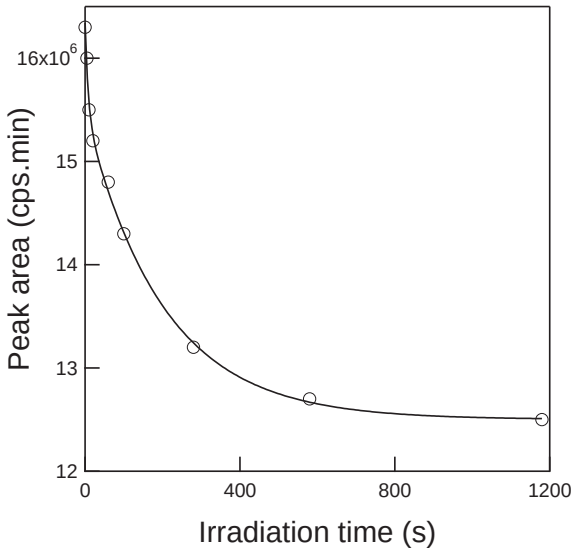

Figure 4S. Temporal evolution of the peak area in the HPLC chromatograms associated to the two stereoisomers of 4-hydroxy-tamoxifen and their corresponding dehydrophenanthrenes after photocyclic rearrangement resulting from illumination with the UV lamp of a 25 μM 4-hydroxy-tamoxifen solution in 1:1 (v:v) acetonitrile:water. Markers: experimental points; solid line: fit $A_0 + A_1 e^{-t/\tau_1} + A_2 e^{-t/\tau_2}$.

In a second experiment, we illuminated with the UV lamp a 25 μM solution of 4-hydroxy-

tamoxifen in 1:1 (v:v) acetonitrile:water for increasing durations. Each extracted aliquot at a given time was subsequently analyzed by HPLC coupled to mass spectrometry. In particular, we specifically analyzed the temporal evolution of the concentration in the compounds exhibiting the molecular weight of the starting 4-hydroxy-tamoxifen. In relation to the reported work on the photodegradation of tamoxifen,[16] those compounds could be the two stereoisomers of 4-hydroxy-tamoxifen and the corresponding dehydrophenanthrenes resulting from a photocyclic rearrangement.[3] The results shown in Figure 4S confirmed the observations by fluorescence emission: 4-hydroxy-tamoxifen is submitted to a photodegradation. We were able to satisfactorily fit the data with a biexponential law yielding two characteristic times: $\tau_1 = 8.0 \pm 3.5$ s and $\tau_2 = 202 \pm 29$ s which could be associated to the photoisomerization and the photocyclization of 4-hydroxy-tamoxifen respectively. In particular, one notices that the longest characteristic time τ_2 is in the same range as the uncaging time measured with the 4,5-dimethoxy-2-nitrobenzyl caging group (~ 300 s; *vide infra*). As we intended to use this photolabile protecting group which proved satisfactory in our previous studies in zebrafish embryos,[14] we decided to adopt 4-hydroxy-cyclofen instead of 4-hydroxy-tamoxifen as an inducer to avoid any significant photodegradation upon uncaging.

[3] All those similar compounds led to the observation of one peak in HPLC. In relation to our purpose, this point is not significant as we were interested in extracting the relaxation times associated to the temporal evolution of the concentrations which are identical for all the species.

Cyclofen-induced control of nuclear translocation in zebrafish embryos

To demonstrate the usefulness of 4-hydroxy-cyclofen (cyclofen) as an analog of 4-hydroxy-tamoxifen, we checked that it could be used to induce the translocation of fluorescent proteins (GFP, reported in the Main Text; mCherry, *vide infra*) fused to the ER^{T2} receptor and possessing a nuclear localization signal (nls).

As shown in Figure 5S, in the absence of inducer, the fluorescence signal from mCherry is distributed throughout the cytoplasm, whereas in the presence of cyclofen, nuclear localization of the fluorescent protein is observed.

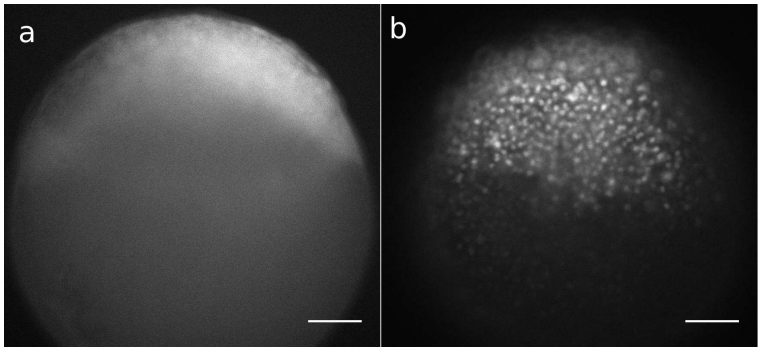

Figure 5S. Cyclofen-OH induction of nuclear translocation of mCherry-nls-ER^T in zebrafish embryos. The wild type embryos were injected with *mcherry-nls-ER^T* mRNA (100 ng/μL) at the one-cell stage and were further incubated with 0 (**a**) or 3 (**b**) μM **Ind**. They were imaged for mCherry-ER^T emission by epifluorescence microscopy at dome stage (same display range in **a** and **b**). Scale bar: 100 μm.

The dose dependence of the GFP-nls-ER^T nuclear translocation on cyclofen concentration is given in Table 2S.

Table 2S. Cyclofen-induced dose effect in zebrafish embryos injected at one cell stage with *gfp-nls-ER^T* (100 ng/μL) mRNA and incubated in various concentrations of inducer. The probability p of observing a positive phenotype is the percentage of embryos exhibiting nuclear localisation of GFP among n embryos investigated. The statistical error is calculated as $\sqrt{p(1-p)/n}$(or $1/n$ when p=0 or 1).

[**Ind**] (μM)	n	p (%)
–	100	12 ± 3
0.3	43	72 ± 7
1	15	86 ± 9
3	52	89 ± 4

Uncaging kinetics of the caged inducers upon UV illumination *in vitro* and *in vivo*

In vitro studies

With the 4 W UV lamp, we illuminated solutions of **cInd**, **c'Ind**, and **c"Ind** in a 1:1 (v:v) acetonitrile:water mixture for increasing durations. Each extracted aliquot at a given time was subsequently stored in the dark and submitted to HPLC analyses following the evolution of the peak area of photoreleased 4-hydroxy-cyclofen **Ind** as a function of the illumination duration.

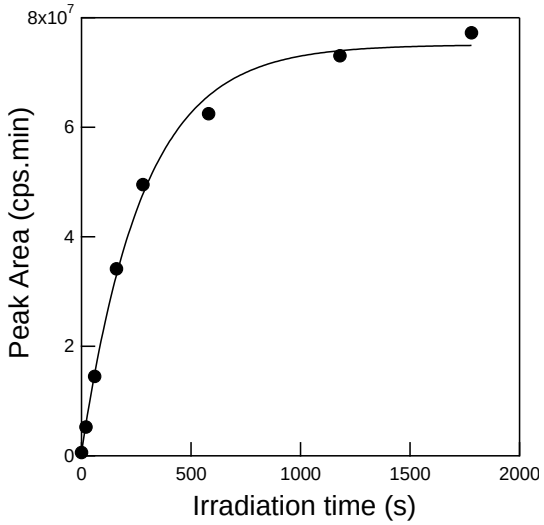

Figure 6S. Evolution of the **Ind** peak area in the HPLC chromatogram resulting from illumination with the UV lamp of a 25 μM **cInd** solution in a 1:1 (v:v) acetonitrile:water mixture. The monoexponential fit $A_0(1-e^{-t/\tau_{UV}})$ displayed as a solid line provides $\tau_{UV} = 280 \pm 30$ s.

Figure 6S displays the result obtained with **cInd**. As anticipated from the first order kinetics of the uncaging reaction for **cInd**, one observes a monoexponential increase of the **Ind** concentration with a characteristic time $\tau_{UV} = 280 \pm 30$ s. In particular, the plateau observed beyond 10^3 s underlines the absence of any photodegradation of 4-hydroxy-cyclofen **Ind** (compare with Figure 4S). We observed under identical illumination conditions a similar monoexponential behavior for the uncaging of **c'Ind** and **c"Ind** with timescales $\tau'_{UV} = 120 \pm 15$ s and $\tau''_{UV} = 620 \pm 60$ s respectively. The observed rate constants were subsequently converted into uncaging cross sections, $\varepsilon_u(365)\Phi_u^{(1)}$, by using Eq.(7) from [17] introducing the values of the geometrical parameters used during illumination ($V = 40$ mL, $l = 6$ mm).

In vivo **studies**

Table 3S displays the probability of nuclear translocation of GFP-nls-ER$^{\mathrm{T}}$ as the duration of UV illumination (i.e. the amount of photoreleased cyclofen) is varied in wild type zebrafish embryos incubated with 3 μM **cInd**.

Table 3S. Dependence of the percentage p of the ligand induced nuclear translocation of GFP-nls-ER$^{\mathrm{T}}$ upon the duration t of UV illumination in wild type zebrafish embryos incubated with **cInd** (3 μM). Table 3S also indicates the total number of investigated embryos n and the number of embryos exhibiting an aberrant development or dead during the assay m. Statistical error is calculated from $\sqrt{p(1-p)/n}$ where p is the percentage of embryos exhibiting a positive phenotype.

t (s)	n	m	p (%)
0	14	1	28 ± 12
30	13	1	54 ± 14
99	15	2	80 ± 10
192	13	2	85 ± 10
447	17	1	94 ± 6

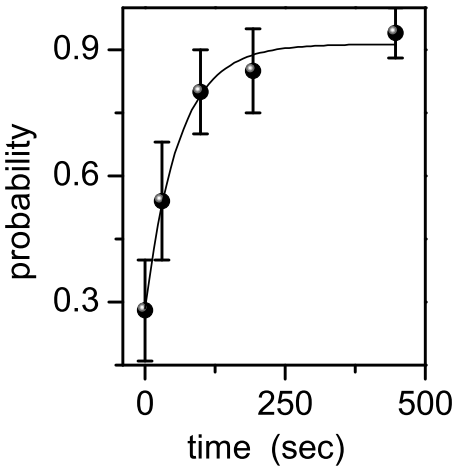

Figure 7S. Dependence of the percentage p of embryos (incubated in 3 μM **cInd**) displaying nuclear localization of GFP-nls-ER$^{\mathrm{T}}$ after a UV illumination of duration t. Dots: Experimental data; Solid line: Exponential fit.

Figure 7S displays the temporal dependence of the percentage p of embryos displaying a nuclear localization of GFP-nls-ER$^{\mathrm{T}}$ following a UV illumination of duration t. Since the uncaging of **cInd** is a first order reaction (Figure 6S), we expect the amount of released inducer to vary as : $Ind(t) = cInd_0[1-\exp(-t/\tau_{UV})]$, where $cInd_0$ is the initial concentration of **cInd**. A fit to the

data in Figure 7S yields $\tau_{UV} = 60 \pm 10$ s in the range observed *in vitro* from HPLC measurements (see above).

In addition, the comparison between the p values at 0.3 and 1 μM **Ind** (see Table 2S) and for illumination durations of 30 and 99 s (expected to photorelease **Ind** at 1 and 2 μM concentration) suggests that the **cInd** concentration within the embryo is in the same range as in the incubating solution.

Uncaging kinetics of cInd with two-photon IR illumination

Measurement of the cInd uncaging cross section with two-photon illumination

To measure the cInd uncaging cross section with two-photon illumination, we illuminated through a 20 × objective (NA 0.75 Nikon) a series of sealed microwells[4] containing a **cInd** solution in 1:1 (v:v) acetonitrile:water at initial concentration $cInd_0 = 1$ μM. The solution stored in each microwell (corresponding to a given illumination time) was submitted to HPLC analyses to determine the concentration of photoreleased 4-hydroxy-cyclofen as a function of the illumination duration.

The uncaging reaction **cInd** $\overset{2h\nu}{\rightarrow}$ **Ind** is considered to take place in a laser illuminated volume $V_{exc} = 8.1$ μm^3 (measured by FCS) at a rate k_{unc}:[18]

$$k_{unc} = 0.737\delta_u \frac{T}{\tau_P}\left(\frac{\lambda}{\pi h c \omega_{xy}^2}\right)^2 P^2 \tag{1}$$

where δ_u is the two-photon uncaging cross section of the 4,5-dimethoxy-2-nitrobenzyl caging group at the excitation wavelength $\lambda = 750$ nm, $T = 13.1$ ns is the period of the laser pulses of incident power $P = 120$ mW, duration $\tau_P = 200$ fs, waist at the focal point $\omega_{xy} = 0.63$ μm (measured by FCS), and h and c are Planck's constant and the speed of light respectively. The uncaging time $\tau_{IR} = V/(k_{unc}V_{exc})$ is larger than the diffusion time $\tau_V \simeq 4\ 10^4$ s in a microwell of volume $V = 3.5$ μL.[5] Thus **cInd** and **Ind** can be considered to be homogeneously distributed within the microwell. Then the dynamics of the concentrations in **cInd** and **Ind**, $cInd$ and Ind, obeys:

$$\frac{dcInd}{dt} = -\frac{dInd}{dt} = -\frac{1}{\tau_{IR}} cInd \tag{2}$$

which can be solved as:

$$Ind(t) - Ind_0 = cInd_0\left(1 - e^{-\frac{t}{\tau_{IR}}}\right) \tag{3}$$

where Ind_0 and $cInd_0$ are the initial concentrations of **Ind** and cInd. For times $t \ll \tau_{IR}$,[6] Eq.

[4] The 3.5 μL microwells were punched in layers of parafilm (~ 1 mm thick; Pechiney Plastic Packaging, Chicago, IL) molten on a ~ 140 μm thick D263 coverslip (Menzel-Gläser, Braunschweig, Germany) with a hot plate at 100°C. After the microwells were filled with the **cInd** solution, watertight sealing was obtained by melting another parafilm layer close to each well with a soldering iron.

[5] τ_{IR} is extracted from the expression (4) whereas an upper estimate of τ_V can be obtained by assuming that mixing within the volume V is controlled by diffusion. Adopting $D = 3.8\ 10^{-12}$ m^{2}s^{-1} (estimated value for Fluorescein at the operating temperature; see [19, 20]) as an order of magnitude of the diffusion coefficient of **cInd** and **Ind**, we derived $\tau_V = (3V/4\pi)^{2/3}/6D = 3.9\ 10^4$ s $< \tau_{IR} = 1.7\ 10^5$ s.

[6] $\tau_{IR} = 1.7\ 10^5$ s is much larger than the investigated uncaging times (40 and 60 min).

(3) becomes

$$Ind(t) - Ind_0 = cInd_0 \frac{t}{\tau_{IR}} = 0.737 \delta_u \frac{T}{\tau_P} \left(\frac{\lambda}{\pi h c \omega_{xy}^2} \right)^2 P^2 \frac{V_{exc}}{V} \; cInd_0 \; t. \tag{4}$$

We measured $Ind_0 = 15$ nM (i. e. 1.5 % of the caged precursor) and $Ind(t) = 28$ nM and 36 nM at $t = 40$ and 60 min of illumination. These data show that two-photon illumination does lead to photorelease of cyclofen from its caged precursor. Moreover, from the observed linear relationship: Ind(nM)$= cInd_0 t/\tau_{IR} + Ind_0 = 0.35 \; t(min)+15$ (R^2=0.998), we derived (using Eq.(4)): δ_u=4 mGM, in reasonable agreement with the values reported for the uncaging cross section of the 4,5-dimethoxy-2-nitrobenzyl caging group for two-photon absorption at a similar wavelength.[17, 21, 22]

Uncaging kinetics of cInd

We already derived the expression of the two-photon uncaging rate in a confined environment of volume V, $\tau_{IR} = V/\left(k_{unc} V_{exc}\right)$. For a cell, $V^{1/3} = 13.5$ μm [14] and using the previously determined value of $\delta_u = 4$ mGM and the $\omega_{xy} = 0.50$ μm and $V_{exc} = 1.7$ μm^3 measured by FCS for the 40× NA=0.8 water immersion objective, we find:

$$\frac{1}{\tau_{IR}(s)} = 2.7 \; 10^2 P^2 \tag{5}$$

At $P = 20$ mW, we obtain $\tau_{IR} = 11$ s for the characteristic two-photon uncaging time for this objective. In this work, the two-photon illumination experiments in single cells were performed at 10–20 mW for typical 10 s times so as to substantially release the caged compound present in the targeted cell.

Kinetics of nuclear translocation

Two series of experiments have been performed to investigate the kinetics of nuclear translocation of GFP-nls-ER$^{\mathrm{T}}$ after **cInd** uncaging.

In Figure 1h, we observed that the average nuclear fluorescence intensity of a cell expressing GFP-nls-ER$^{\mathrm{T}}$ increases exponentially upon targeted cyclofen photorelease with a typical time scale $t_n = 1000 \pm 300$ s.

We also used Fluorescence Correlation Spectroscopy (FCS) to analyze the kinetics of GFP nuclear translocation by recording the FCS signal in the cytoplasm of a CV1 cell (transfected with GFP-nls-ER$^{\mathrm{T}}$ expression plasmid and incubated in 6 μM **cInd**) at various times after UV laser illumination (similar FCS curves where obtained when two-photon illumination was used). Figure 8S displays a series of FCS data obtained at 200 s intervals.

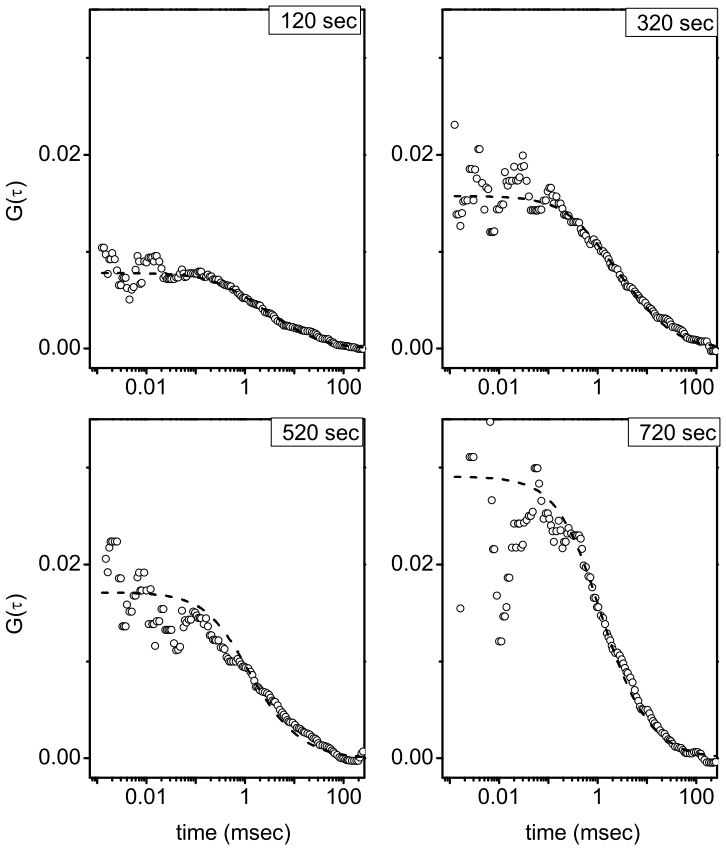

Figure 8S. Time-series of the FCS curves of cytoplasmic GFP recorded (at $\lambda_{exc} = 488$ nm) at different times (200 s between successive FCS curves) after uncaging 6 μM **cInd** with a 5 s UV laser illumination pulse. Dots: Experimental points; Dashed line: Best fit to a two-species (6) model (GFP bound to cytoplasmic chaperones or not) with diffusion coefficients D_1 and D_2.

The FCS curves have been globally analyzed as a function of the time t after cyclofen release by adopting a model where the illumination volume is assumed to contain two fluorescent species with diffusion constant D_i $(i = 1, 2)$: a GFP-nls-ER$^{\mathrm{T}}$ unbound state **1** and a chaperone bound complex **2**.[7] The FCS curve can then be written as:

$$G(\tau) = \Sigma_{i=1}^{2} \left(\frac{\mathcal{Q}_i \overline{N_i}}{\Sigma_{i=1}^{2} \mathcal{Q}_i \overline{N_i}} \right)^2 G_i(\tau, N_i, \tau_i) \tag{6}$$

with:

$$G_i(\tau, N_i, \tau_i) = \frac{1}{\overline{N_i}} \left(1 + \frac{\tau}{\tau_i} \right)^{-1} \left(1 + \omega^2 \frac{\tau}{\tau_i} \right)^{-\frac{1}{2}} \tag{7}$$

where $\overline{N_i}$ is the average number of molecules in state i contained in the illumination volume, $\mathcal{Q}_i$ and $\tau_i (= \omega_{xy}^2 / 8D_i)$ their brightness and diffusion time through the beam waist (ω_{xy}) and $\omega = \omega_z / \omega_{xy}$ the aspect ratio of the illuminated volume.

Satisfactory fits were obtained with various (τ_1,τ_2) combinations without significantly altering characteristic decay times (*vide infra*). To reduce uncertainties, we fixed $\tau_1 = 1.7$ ms, a value contained in the range allowed by the previous fits and derived for GFP-nls-ER$^{\mathrm{T}}$ from the GFP diffusion coefficient (25 μm^{2}s^{-1}; [23]) by taking into account the difference of molecular weights (66.6 kDa for GFP-nls-ER$^{\mathrm{T}}$ and 27 kDa for GFP). Then we performed a satisfactory global fit of the whole series of FCS autocorrelation curves (see Figure 8S).

From these fits the values of $G_i(\tau = 0, t) = \frac{\mathcal{Q}_i^2 \overline{N_i}(t)}{\left(\mathcal{Q}_1 \overline{N_1}(t) + \mathcal{Q}_2 \overline{N_2}(t) \right)^2}$ at various times t were determined. It turns out that the ratio $G_1(0,t)/G_2(0,t)$ is constant (see Figure 9Sb) which implies that the ratio of bound to unbound species is also constant. We thus deduced that the equilibrium between these two states occurs on a time scale faster than the one associated to nuclear translocation. We correspondingly observed similar characteristic times associated to the exponential increase of $G_i(0,t)$ (see Figure 9S). From $G_1(0,t) + G_2(0,t)$ which is inversely proportional to the number of cytoplasmic GFP-nls-ER$^{\mathrm{T}}$ molecules, we eventually deduced that nuclear translocation happens on a time scale $t_n = 450 \pm 20$ s, in the range observed for the measurements of nuclear fluorescence increase.

From the diffusion times $\tau_1 = 1.7$ ms and $\tau_2 = 240$ ms, we deduced the corresponding diffusion coefficients for the unbound and bound species: $D_1 = 18.5\ \mu m^2 s^{-1}$ and $D_2 = 0.1\ \mu m^2 s^{-1}$. In

[7] In all investigated cases, a global fit of the FCS curves to a one species diffusion model was poor.

particular, D_2 is significantly smaller than D_1 as anticipated from the formation of a large complex between GFP-nls-ER$^{\mathrm{T}}$ and the chaperone complex.

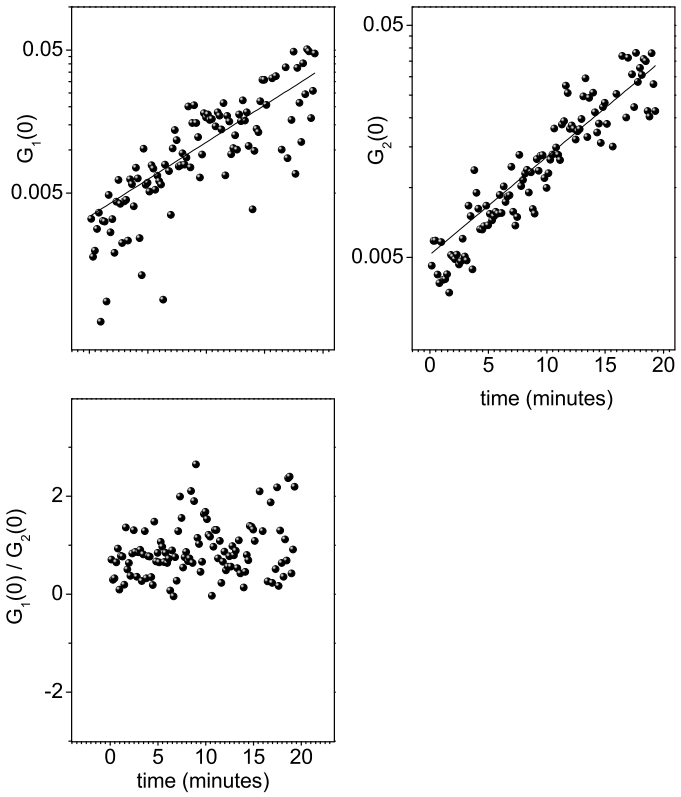

Figure 9S. Analysis of the FCS data displayed in Figure 8S: Time dependence of $G_1(\tau = 0, t)$, $G_2(\tau = 0, t)$, and of the ratio $G_1(\tau = 0, t)/G_2(\tau = 0, t)$ extracted from a two-species model with τ_1= 1.7 ms and τ_2= 240 ms. Dots: Experimental points. Solid line: Fit to an exponential decrease of the cytoplasmic species (due to nuclear translocation).

Colocalization experiment with local UV illumination

To demonstrate that the induction of protein activity upon cyclofen uncaging occurs in the targeted illuminated cells, we used a UV laser (5 μW) to perform a local photoactivation (for 5 s) of **cInd** and caged fluorescein dextran (**cFd**) in embryos injected at the one cell stage with **cFd** and *gfp-nls-ER^T* mRNA and incubated in embryo medium supplemented with 3 μM **cInd**. From the different emission spectra of GFP and Fluorescein, their contributions to the fluorescence signal can be separated by analyzing images recorded at different wavelengths. Figures 10Sa–c display the images of a zebrafish embryo (60 min after illumination) obtained from recording the emission from GFP, Fluorescein, and both fluorophores respectively. One notices the cytoplasmic localization of fluorescein in the same cells in which the GFP-nls-ER$^{\mathrm{T}}$ signal is predominantly localized in the nucleus.

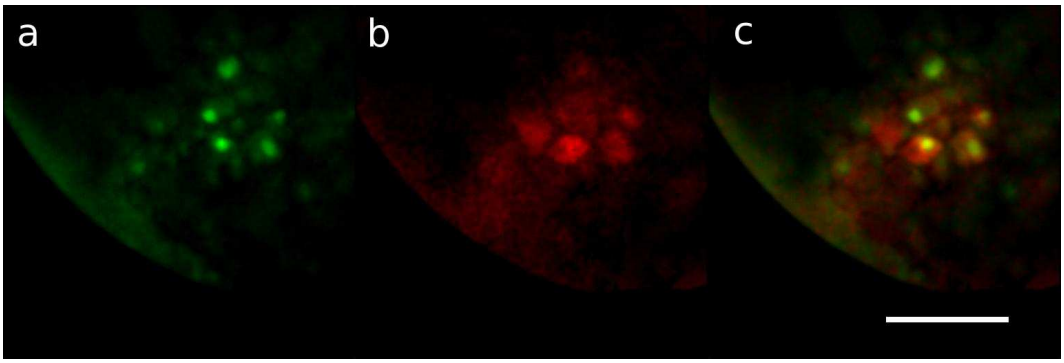

Figure 10S. Images resulting from local photoactivation of GFP-nls-ER$^{\mathrm{T}}$ in a wild type embryo injected with *gfp-nls-ER^T* mRNA and caged fluorescein dextran at one-cell stage and conditioned as in Figure 2**d**–**e**. Emission from GFP (**a**), Fluorescein (**b**), and both fluorophores (**c**) respectively. Scale bar: 100 μm.

References

[1] F. F. Vajdos, L. R. Hoth, K. F. Geoghegan, S. P. Simons, P. K. LeMotte, D. E. Danley, M. J. Ammirati, J. Pandit, *Protein Sci*, **2007**, *16*, 897–905.

[2] E. Krieger, T. Darden, S. B. Nabuurs, A. Finkelstein, G. Vriend, *Proteins*, **2004**, *57*, 678–683.

[3] J. Wang, P. Cieplak, P. A. Kollman, *J. Comput. Chem.*, **2000**, *21*, 1049–1074.

[4] W. Humphrey, A. Dalke, K. Schulten, *J. Mol. Graph.*, **1996**, *14:33–38*, 27–38.

[5] Gromacs (http://www.gromacs.org).

[6] R Development Core Team, R: A Language and Environment for Statistical Computing, Vienna, Austria, **2007**.

[7] Grace (http://plasma-gate.weizmann.ac.il/Grace/).

[8] H. J. Montgomery, B. Perdicakis, D. Fishlock, G. A. Lajoie, E. Jervis, J. G. Guillemette, *Bioorg Med Chem*, **2002**, *10*, 1919–1927.

[9] T. Eckardt, V. Hagen, B. Schade, R. Schmidt, C. Schweitzer, J. Bendig, *J Org Chem*, **2002**, *67*, 703–710.

[10] M. M. Cid, J. A. Seijas, M. C. Villaverde, L. Castedo, *Tetrahedron*, **1988**, *44*, 6197–6200.

[11] S. D. Lepore, Y. He, *J Org Chem*, **2003**, *68*, 8261–8263.

[12] A. Z. Suzuki, T. Watanabe, M. Kawamoto, K. Nishiyama, H. Yamashita, M. Ishii, M. Iwamura, T. Furuta, *Org Lett*, **2003**, *5*, 4867–4870.

[13] O. Krichevsky, G. Bonnet, *Rep. Prog. Phys.* **2002**, *65*, 251–297.

[14] P. Neveu, I. Aujard, C. Benbrahim, T. Le Saux, J.-F. Allemand, S. Vriz, D. Bensimon, L. Jullien, *Angew. Chem. Int. Ed.*, **2008**, *47*, 3744–3746.

[15] K. H. Link, Y. Shi, J. T. Koh,*J. Am. Chem. Soc.*, **2005**, *127*, 13088–13089.

[16] J. Salamoun, M. Macka, M. Nechvatal, M. Matousek, L. Knesel, *J. Chrom.*, **1990**, *514*, 179–187.

[17] I. Aujard, C. Benbrahim, M. Gouget, O. Ruel, J. B. Baudin, P. Neveu, L. Jullien, *Chem. Eur. J.*, **2006**, *12*, 6865–6879.

[18] N. Kiskin, R. Chillingworth, J. A. McCray, D. Piston, D. Ogden, *Eur. Biophys. J.*, **2002**, *30*, 588–604.

[19] A. Estévez-Torres, C. Gosse, T. Le Saux, J.-F. Allemand, V. Croquette, H. Berthoumieux, A. Lemarchand, L. Jullien, *Anal. Chem.*, **2007**, *79*, 8222–8231.

[20] Z. Petrásek, P. Schwille, *Biophys. J.*, **2008**, *94*, 1437–1448.

[21] T. Furuta, S. S.-H. Wang, J. L. Dantzker, T. M. Dore, W. J. Bybee, E. M. Callaway, W. Denk, R. Y. Tsien, *Proc. Nat. Acad. Sci. USA*, **1999**, *96*, 1197–1200.

[22] E. B. Brown, J . B. Shear, S. R. Adams, R. Y. Tsien, W. W. Webb, *Biophys. J.*, **1999**, *76*, 489–499.

[23] Y. Chen, J. D. Müller, Q. Q. Ruan, E. Gratton, *Biophys. J.*, **2002**, *82*, 133–144.